國 立 交 通 大 學

光 電 工 程 研 究 所

碩 士 論 文

氧化銦錫薄膜與奈米結構兆赫頻段
光學特性之研究

Terahertz spectroscopic studies of
ITO thin films and nanostructures

研 究 生：林晏徵

指導教授：潘犀靈 教授

中 華 民 國 九 十 八 年 七 月

氧化銦錫薄膜與奈米結構兆赫頻段光學特性之研究

Terahertz spectroscopic studies of ITO thin films and nanostructures
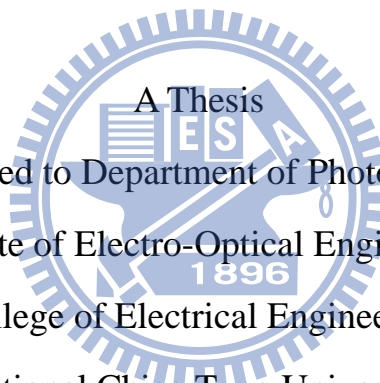
學生：林晏徵   Student: Yen-Cheng Lin

指導教授：潘犀靈教授   Advisor: Prof. Ci-Ling Pan

國立交通大學

光電工程研究所

碩士論文

A Thesis

Submitted to Department of Photonics and

Institute of Electro-Optical Engineering

College of Electrical Engineering

National Chiao Tung University

In partial Fulfillment of The Requirements

For The Degree of Master of Science

In

Electro-Optical Engineering

July 2009

Hsinchu, Taiwan, Republic of China

中華民國九十八年七月

氧化銦錫薄膜與奈米結構兆赫頻段光學特性之研究

學生：林晏徵　　　　　　　　　　　　　　指導教授：潘犀靈教授

國立交通大學研究所

摘要

我們使用富立業遠紅外光光譜以及兆赫波時域光譜的光學量測方法去探討氧化銦錫薄膜及氧化銦錫奈米柱的光學特性和電性。且對於不同厚度的薄膜(189nm ~ 961nm)，我們得到以下的特性：

樣品之電漿頻率隨著厚度變厚而變大，其值 1600(rad.THz)到 1950(rad.THz)。以 Drude 的自由載子模型的知載子散射時間為 6～7(fs)。且我們也同樣得到對應的載子漂流率跟載子濃度，分別為 32～34(cm^2/Vs)和(2.8～4.2)$\times 10^{20}$。我們得到的這些電性結果可以跟霍爾量測到的結果做相對應的比較，且得到相近的數值。

同樣的，我們可以將這光學量測技術使用於奈米結構樣品的探討。在本論文裡面，我們將研究氧化銦錫的奈米柱結構，並引進 Drude-Smith 模型及等校介值理論來輔助分析。

Terahertz spectroscopic studies of ITO thin films and nanostructures

Student: Yen-Cheng Lin   Advisor: Prof. Ci-Ling Pan

Department of Photonics and Institute of Electro-Optic Engineering, College of

Electrical Engineering National Chiao Tung University

Abstract

We investigate the optical and electrical properties of Indium Tin Oxide (ITO) thin film and Indium Tin Oxide (ITO) nanocolumns with the optical characterization methods including Fourier Transform Infrared Spectroscopy (FTIR) and Terahertz Time Domain Spectroscopy (THz-TDS). For different thicknesses of the Indium Tin Oxide (ITO) thin films (189nm~961nm), the plasma frequencies are determined to be from 1600 (rad.THz) to 1950 (rad.THz), and scattering times are in the range of 6~7 fs based on the free electron Drude model. The mobilities of the above Indium Tin Oxide (ITO) thin films are determined to be $32\sim34\text{cm}^2$/Vs. The carrier concentration is verified to be in the range of $(2.8\sim4.2)\times10^{20}$. The electrical properties of the thin films derived from non-contact optical techniques agree well with those determined by the conventional Hall measurement.
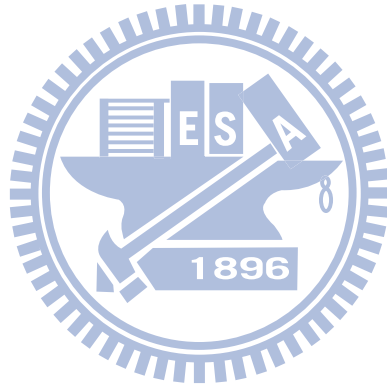
Similarly, the techniques are also introduced to the nanostructure materials, Indium Tin Oxide (ITO) nanocolumn. We study the optical and electrical properties of the sample with the Drude-Smith model and the effective medium approximation (EMA) which are demonstrated in the thesis.

致謝

兩年的碩班生活即將結束了！在這要先感謝一起修課的同學們，沒有你們的陪伴，我是當不了早起的鳥兒的。因為有你們，我的修課生活變得很精彩。

就算畢業了，也一定不會忘記實驗室的同仁們的，因為大家給的指導跟關心，是我做研究得動力。且這篇碩論之所以能完成，完全都要感謝 Moya 學長亦師亦友的指導，以及 Mika 學長的經驗傳承跟 Tiger 的問題討論，還有山哥及猛哥的巧手教學及冠儒學弟的實驗幫忙等等。沒有你們或許我會念碩士真得要念碩四了！

最後要感謝的是我的家人，沒有你們的支持，我想我是很難度過最後難關的。尤其是妹妹芝嶸更是在我百忙之際時雪中送炭！謝謝你們，最愛你們了！

Contents

Chapter 1 Introduction

Chapter 2 Models and Analysis Methods

Chapter 3   Experimental Result and Discussion of ITO Thin Film

Chapter 4   Experimental Result of ITO nanocolumn

Chapter 5

List of Figures

List of Tables

Chapter 1 : Introduction

1-1   Introduction of THz

Terahertz (THz) radiation lies in the frequency gap between the infrared and microwaves(see Fig. 1-1-1), typically is referred to as the frequencies from 100 GHz to 30 THz. 1 THz is equivalent to 33.33cm^{-1} (wave numbers), 4.1 meV photon energy, 300μm wavelength. Before 1980s people don't know much about THz because the generation and detection technologies are not well established, but since the development of femtosecond laser, THz has been intensely studies. At middle 1980s, Auston [1] successfully used photoconductive dipole antenna to generate and detect coherently THz radiation in time domain, and this technology is called THz time-domain spectroscopy (THz-TDS). After Auston's research many other generation methods have been developed including optical rectification [2], surge current in semiconductor surface [3], quantum cascade laser [4]…, and in 1995 XC-Zhang *et al*[5] successfully used ZnTe crystal to detect THz radiation by free-space electro-optic sampling that highly increased the detection bandwidth and signal to noise ratio.
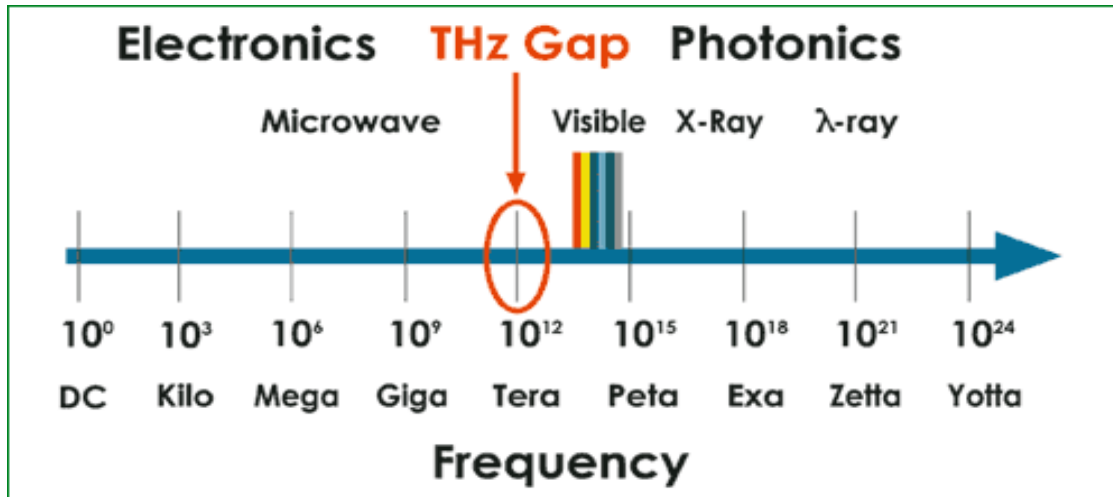
Fig.1-1-1 The spectral range of electromagnetic waves
(http://www.rpi.edu/terahertz/about_us.html)

Terahertz has much smaller photon energy (4.1 meV) compared to X-ray and therefore this kind of non-destruction measurement can be used for biology and medical sciences [6]. Image and tomography [7] of THz have also been studied and can be applied to homeland security.

For semiconductors measurement, conventional four point probe and Hall effect measurement can measure the characteristics including mobility, carrier concentration and resistivity of the semiconductor materials by direct sample contact. All these electrical measurements measure only DC value of the sample but some characteristics, including refractive index, conductivity, are frequency-dependent. For some semiconductors with high resistivity and low concentration, the electrical properties are difficult to be measured by simple direct contact because at the metal-semiconductors interface, the Schottky barrier may disturb the measurement value. Therefore, THz-TDS with advantages of non-contact and frequency-dependant measure is desirable for semiconductors characterization. In 1990 D. Grischkowsky *et al* [8] successfully measured optical properties including refractive index and conductivity of GaAs wafer and the results fit well with the Drude model. Besides

2

GaAs, other semiconductors such as silicon [9] have also been widely studied. Recently, many nanostructured semiconductors like InP-nanoparticle [10], ZnO-nanowire [11], Si-nanoparticle [12] have been studied using THz-TDS technology and the particular conduction behavior have been observed. In comparison with conventional far-IR source and detector, THz-TDS is a coherent technology that means both amplitude and phase information can be obtained. Both absorption coefficient and refractive index could be extracted without use of Kramers-Kronig relation that simplifies the analysis process.

1-2   Transparent Conductive Oxides (TCOs)

Basic introduction of PV Solar Cell

Nowadays, solar cells have become essential devices because of the energy crisis. The major and subsequence field of studying solar modules become the top topic of the Green-energy because of the shortage of petroleum and coal which are the powerful and useful energy sources creating a successfully prosperous industry world in nineteenth and twentieth century.

The quest for low-cost, high-effective, sustainable energy source is one of the prior concerns of the industrial society at the present age. Photovoltaic solar energy is the major part in this quest. The main reason is related to their manufacturing cost, to their market price. This kind of thin film photovoltaic solar cell can be deposited on low-cost large-area substrates. Various semiconductors, compound semiconductors, have been invested for thin film solar cell such as CdTe and Cu (In, Ga)Se2 (CIGS) have attracted much attention in the past research, because of relatively high laboratory efficiencies. For the low cost purpose, the thin film silicon solar cell manufacturing is the best choice.

TCOs of PV Solar Modules

Thin film silicon solar cells, consisting of amorphous and microcrystalline silicon which have the relatively low value of absorption coefficient, need elaborate light-trapping schemes in order to absorb a sufficient part of incoming solar spectrum, within reasonable thickness to ensure satisfactory efficiencies. In a solar cell, to increase the photo-generation and short circuit current density, all reflection and absorption losses have to be minimized. It means as below:

(a.) AR coating might be used on the solar module where light enters into it.

(b.) Back reflectors necessarily have as little absorption as possible

(c.) The substrate and the front TCO layer must have high transparency at 300 to 1200 nm, the solar spectral range.

(d.) TCO layers and the layers which do not contribute to photo-generation and collection, should be kept as thin as possible and have very low absorption coefficient in the acting spectral range.
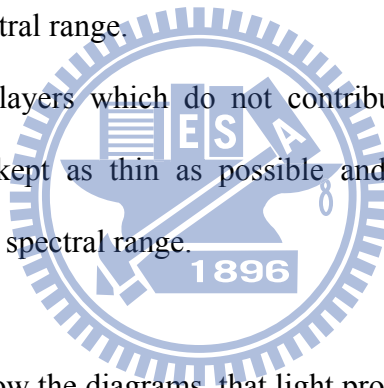
Fig. 1-2-1 and 1-2-2 show the diagrams, that light propagate in the solar cell. With the rough surface of the TCO layers, the sunlight is widely scattered and improving the absorption at the silicon layers which transverse the light energy to the electrical energy. And in the diagram, it also shows the benefit of the back reflector, which reflects the light to confine the propagating light. [13][14]
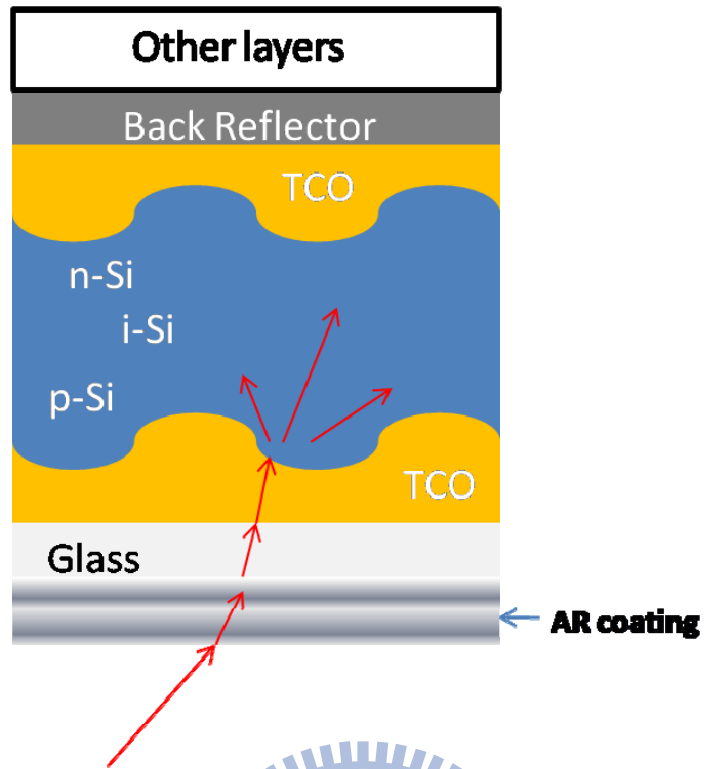
Fig. 1-2-1 The p-i-n type thin film silicon solar cell with light incident
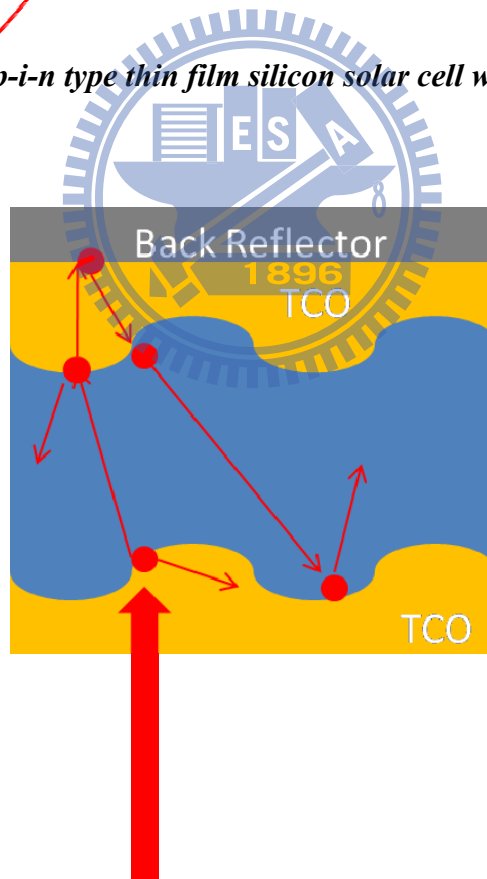
Fig. 1-2-2 Rough surface of TCO and back reflector to increase the light absorption

TCO layers are used as a front electrode and as part of the back side reflector in the solar module. When it applied at the front side, there are few properties should followed:

(a.) High transparency (in the spectral rang where solar cell is operating).

(b.) High conductivity

(c.) Strong scattering of the incoming light into Si absorber layer.

(d.) To be favorable physical-chemical properties for the growth of the silicon.

ITO Film from NDL:

ITO thin films with thickness as followed, 961.6nm, 483.0nm, and 188.9nm, are prepared by NDL with the DC reactive magnetron sputtering. The growth conditions are shown below:

1. vacuum pressure: 6 m-torr

2. sputtering power: 300W

3. growth on fused silica, the substrate

4. substrate temperature: $250^{\circ}C$

5. with O_2 and Ar
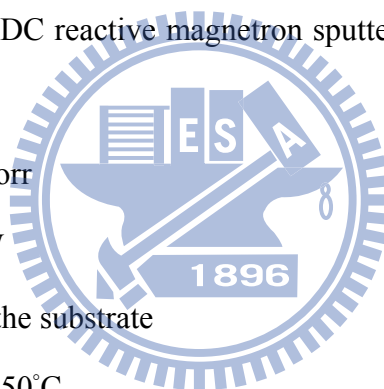
By using the commercial machine, Ulvac DC sputter, with target compositions are 90 wt% In_2O_3 +10 wt% SnO_2 and purity of it is 99.99 wt% manufactures the ITO thin films.

The morphology of the ITO thin film: (the surface roughness and the grain)

Fig. 1-2-3 ~ 1-2-5 are shown in the SEM photography.
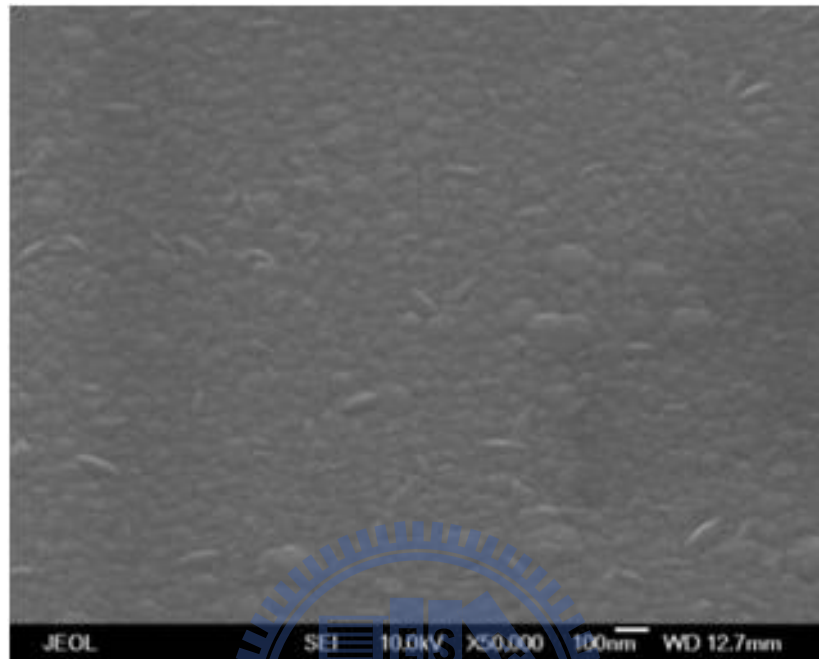
Fig. 1-2-3 Film with thickness 961.6(nm)
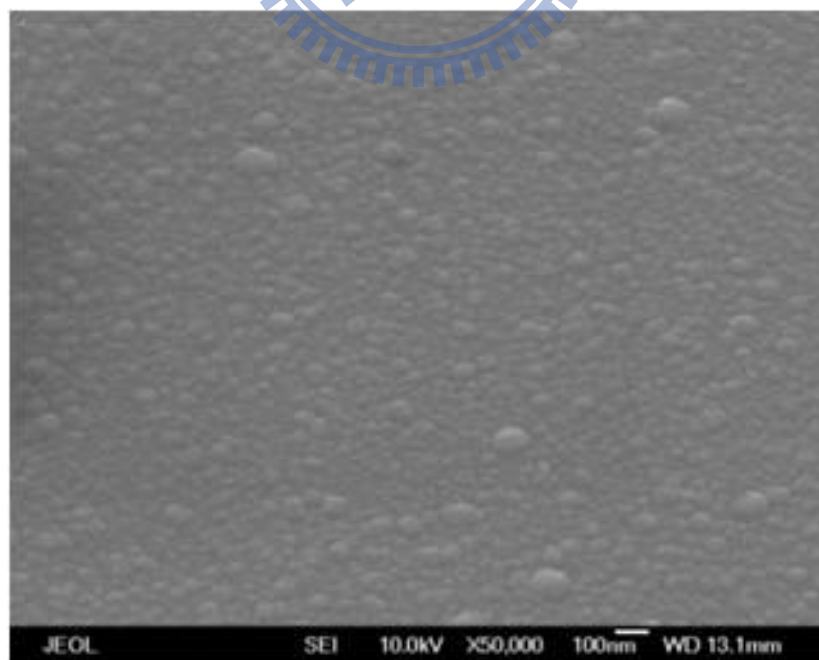
Fig. 1-2-4 Film with thickness 483.0(nm)
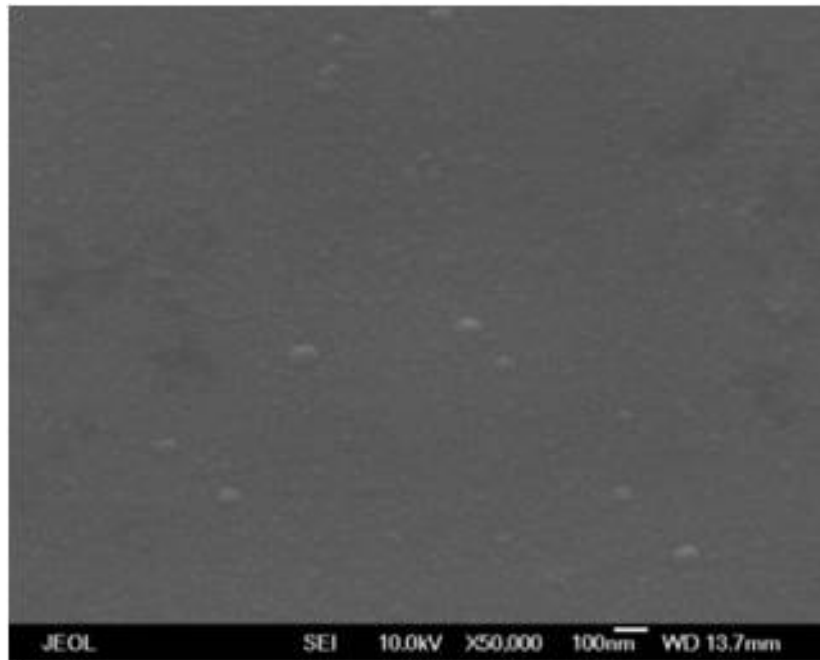
Fig. 1-2-5 Film with thickness 188.9(nm)

The Fig.1-2-3 to 1-2-5 show the top views of our ITO film samples. The magnification is ×50,000. The pictures with a scale 100nm make us find out the grain size of each sample. Therefore, we have the grain size, 30nm, 20nm, 10nm for the sample with thickness, 961.6nm, 483.0nm, 188.9nm, respectively.

ITO Nanocolumn from Prof. Yu

ITO nanoculumn with thickness 1μm is grown under the following conditions:

1. deposition angle: $\alpha \sim 70°$

2. vacuum pressure: 10^{-4} torr

3. growth on Si cell

4. substrate temperature: $240°C$

5. with N_2

Using the commercial target compositions are 95 wt% In_2O_3 + 5 wt% SnO_2.

The chamber diagrams are shown below: Fig.1-2-6 and Fig.1-2-7
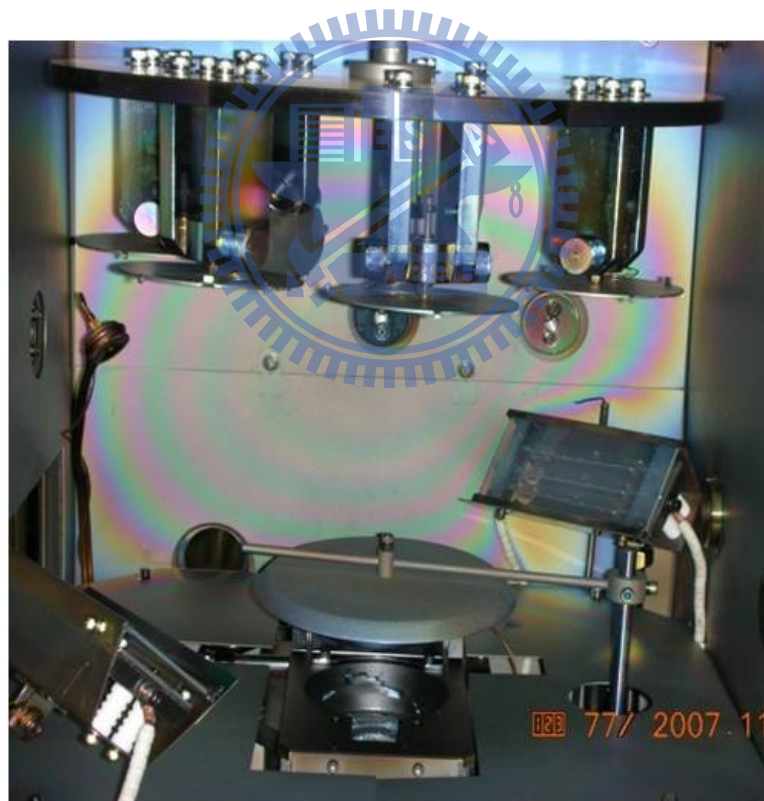
Fig. 1-2-6 The picture of the chamber
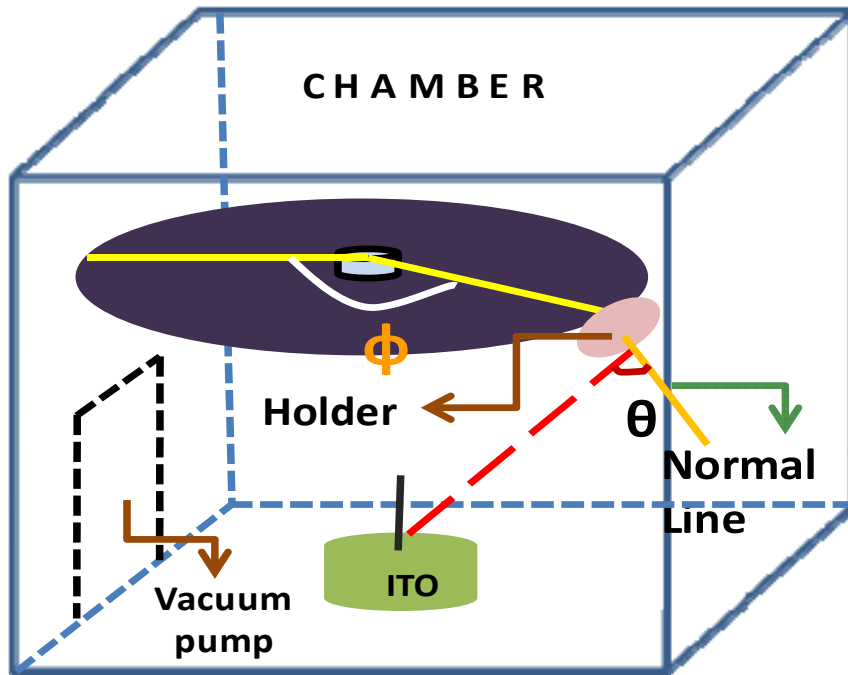
Fig. 1-2-7 A cutaway view of the chamber
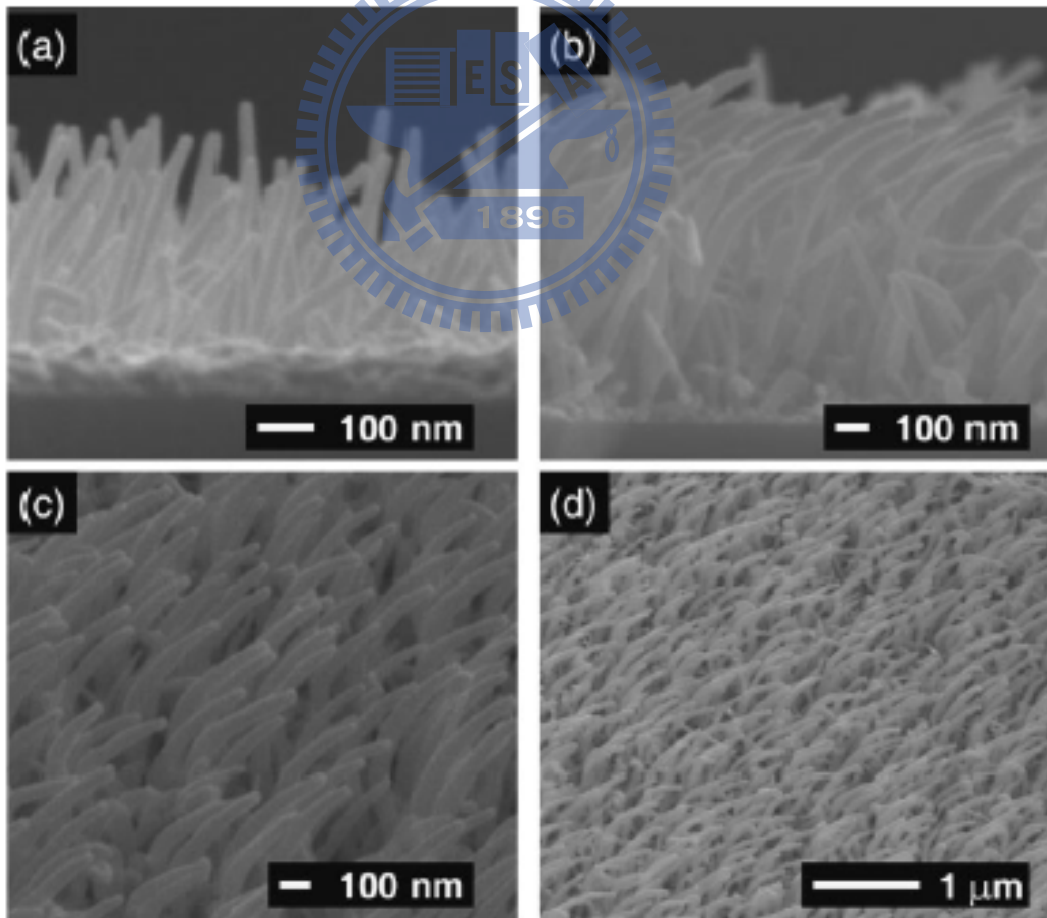
Fig. 1-2-8 SEM image of ITO nanocolumns deposited with obliquely incident with nitrogen flux [15]

1-3   Motivation

The THz region is ideal for probing semiconductors because the frequency range closely matches typical carrier scattering rates of 10^{12} to 10^{14} (Hz).

Therefore, we introduce the optical characterization techniques including FTIR and THz-TDS to measure our samples, ITO thin films and ITO nanocolumn, prepared by NDL and Prof. Yu's group, respectively. It is a non-contact probe method that could avoid destroying our sample surface. By optical analysis with Drude and Drude Smith model, we also could get the electric properties, such as DC mobility, DC conductivity and carrier concentration.

We will introduce the effective medium theory to the nanostructure sample. In the scale around the atom site, the localized field cannot be ignored. And it is a very interesting topic for the physical phenomenon.
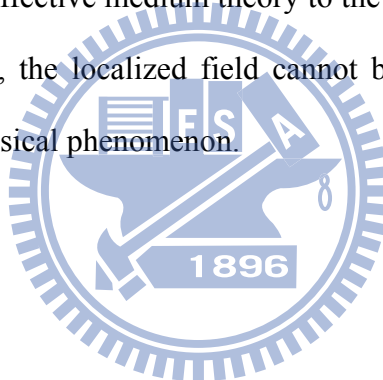
Chapter 2 : Theoretical and experimental methods

2-1　Analysis Models

Macroscopic Fields and Maxwell's Equations:

The electromagnetic state of matter at a given point is described by four quantities:

(1). the volume density of electric charge ρ

(2). the volume density of electric dipoles, called the polarization **P**

(3). the volume of density of magnetic dipoles, called the magnetization **M**

(4). the electric current per unit area, called the current density **J**

All of these quantities are considered to be macroscopically averaged to smooth out the microscopic variations due to the atomic makeup of all matter. The relations of the macroscopically averaged field E and H are described as following by Maxwell equations:

- $\nabla \times \vec{\mathrm{E}} = -\mu_0 \dfrac{\partial \vec{H}}{\partial t} - \mu_0 \dfrac{\partial \vec{M}}{\partial t}$ $\qquad => \nabla \times \vec{\mathrm{E}} = -\dfrac{\partial \vec{B}}{\partial t}$ $\quad$ --- (2-1-1)

- $\nabla \times \vec{\mathrm{H}} = \varepsilon_0 \dfrac{\partial \vec{\mathrm{E}}}{\partial t} + \dfrac{\partial \vec{\mathrm{P}}}{\partial t} + \vec{\mathrm{J}}$ $\qquad => \nabla \times \vec{\mathrm{H}} = \dfrac{\partial \vec{D}}{\partial t} + \vec{J}$ $\quad$ --- (2-1-2)

- $\nabla \bullet \vec{\mathrm{E}} = -\dfrac{1}{\varepsilon_0} \nabla \bullet \vec{P} + \dfrac{\rho}{\varepsilon_0}$ $\qquad => \nabla \bullet \vec{\mathrm{D}} = \rho$ $\qquad$ --- (2-1-3)

- $\nabla \bullet \vec{H} = -\nabla \bullet \vec{M}$ $\qquad => \nabla \bullet \vec{\mathrm{B}} = 0$ $\qquad$ --- (2-1-4)

$\vec{D} = \varepsilon_0 \vec{E} + \vec{P} = \varepsilon \vec{E}$, called the electric displacement --- (2-1-5)

$\vec{B} = \mu_0 (\vec{H} + \vec{M}) = \mu \vec{H}$, called the magnetic induction --- (2-1-6)

In our case, we separate bound charge and bound current from free charge and free current. This separation is more useful for calculations involving dielectric materials.

- $\nabla \times \vec{E} = -\dfrac{\partial \vec{B}}{\partial t}$ --- (2-1-7)

- $\nabla \times \vec{H} = \dfrac{\partial \vec{D}}{\partial t} + \vec{J}_f$ --- (2-1-8)

- $\nabla \bullet \vec{D} = \rho_f$ --- (2-1-9)

- $\nabla \bullet \vec{B} = 0$ --- (2-1-10)

Propagation of Light in Isotropic Dielectrics: [16]

The electrons are permanently bound to the atoms comprising the medium of a non-conducting, isotropic medium. Assume that each electron, of charge -e, has a displaced distance **r** from its equilibrium position. The macroscopic polarization **P** of medium is given by **P** = -*N*e**r**, where *N*(tilted) is the number of electrons per unit volume. Apply a static electric field **E**, the restoring force of electron is –e**E**=κ**r**. If the electric field varies with time, the motion of equation with the damping term is

$-e\vec{E} - \kappa \vec{r} - m\gamma \dot{\vec{r}} = m\ddot{\vec{r}};$

$\Rightarrow -e\vec{E} = (-\omega^2 m - i\omega m\gamma + \kappa)\vec{r};$ --- (2-1-11)

Consequently, the polarization is given by

$$\vec{P}=-Ne\vec{r} = \frac{Ne^2}{-m\omega^2 - i\omega m\gamma + \kappa}\vec{E} = \frac{Ne^2/m}{\omega_0^2 - \omega^2 - i\omega\gamma}\vec{E}; \quad \omega_0 = \sqrt{\frac{\kappa}{m}}, \quad \text{--- (2-1-12)}$$

where ω_0 is the effective resonance frequency of bound electrons.

To show how the polarization affects the propagation of the light, we return the the general wave equation derived from Maxwell's equation.

$$\nabla \times (\nabla \times \vec{E}) + \frac{1}{c^2}\frac{\partial^2 \vec{E}}{\partial t^2} = -\mu_0 \frac{\partial^2 \vec{P}}{\partial t^2} - \mu_0 \frac{\partial \vec{J}}{\partial t}, \quad \text{--- (2-1-13)}$$

In the above wave equation, the polarization term is important for non-conductive medium. On the other hand, the conduction term dominates for the metals. Considering $\nabla \cdot E = 0$ and equation 2-1-13, we have

$$\nabla^2 \vec{E} = \frac{1}{c^2}(1 + \frac{Ne^2}{m\varepsilon_0}\frac{1}{\omega_0^2 - \omega^2 - i\gamma\omega})\frac{\partial^2 \vec{E}}{\partial t^2}; \quad \text{--- (2-1-14)}$$

To seek a solution of the form

$$\left[\vec{E} = \vec{E}_0 e^{i(\widetilde{K}z - \omega t)} \right].$$

It's called homogeneous plane harmonic waves.

The possible solution is provided

$$\widetilde{K}^2 = (\frac{\omega}{c})^2(1 + \frac{Ne^2}{m\varepsilon_0}\frac{1}{\omega_0^2 - \omega^2 - i\gamma\omega}); \quad \left[\widetilde{K} = \frac{\omega}{c}\widetilde{N} \right].$$

$$\Rightarrow \widetilde{N}^2 = (n + i\kappa)^2 = 1 + \frac{Ne}{m\varepsilon_0}(\frac{1}{\omega_0^2 - \omega^2 - i\gamma\omega}). \quad \text{--- (2-1-15)}$$

Propagation of Light in Conducting Media: (free electron gas) [16]

Since the conduction electrons are not bound, there is no elastic force involved. We only consider the electron scattering inside the motion of equation as the form:

$$m\frac{d\vec{v}}{dt} + m\tau^{-1}\vec{v} = -e\vec{E}$$ ($m\tau^{-1}$ is the frictional dissipation constant) --- (2-1-16)

The current density is **J**=-N*e***v**, *N* is the number of conduction electrons per unit volume. The equation can be derived as followed:

$$\frac{d\vec{J}}{dt} + \tau^{-1}\vec{J} = \frac{Ne^2}{m}\vec{E}$$ --- (2-1-17)

(1.) Homogeneous solution:

$$\frac{d\vec{J}}{dt} + \tau^{-1}\vec{J} = 0,$$

The solution of it is:

$\vec{J} = \vec{J}_0 e^{-t/\tau}$, τ is called the relaxation time.

For a static electric field,

$$\tau^{-1}\vec{J} = \frac{Ne^2}{m}\vec{E}$$ (**J**=σ_0**E**), $\sigma_0 = \frac{Ne^2}{m}\tau$;   --- (2-1-18)

(2.) With harmonic time variation field **E** ($e^{-i\omega t}$):

$$(-i\omega+\tau^{-1})\vec{J} = \frac{Ne^2}{m}\vec{E} = \tau^{-1}\sigma_0\vec{E},$$

From above equation we get the current density as the form:

$$\vec{J} = \frac{\sigma_0}{1-i\omega\tau}\vec{E},$$

Here we also introduce **J**=σ**E** in our assumption. We have

$$\sigma(\omega)=\frac{\sigma_0}{1-i\omega\tau};$$ (It's the well-known Drude formula.) --- (2-1-19)
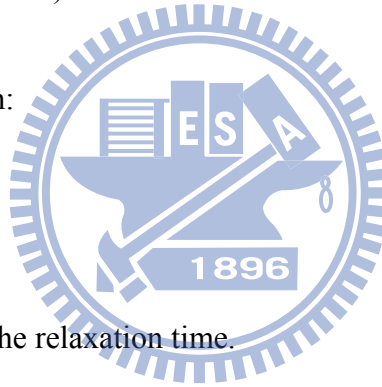
We also introduced the result to the general wave equation, and the equation is reduced to

$$\nabla^2 \vec{E} = \frac{1}{c^2}\frac{\partial^2 \vec{E}}{\partial t^2} + \frac{\mu_0 \sigma_0}{1-i\omega\tau}\frac{\partial \vec{E}}{\partial t}; \quad \text{--- (2-1-20)}$$

We also take the simple homogeneous plane-wave solution as our trial solution.

$$\left[\vec{E} = \vec{E}_0 e^{i(\widetilde{K}z - \omega t)}\right].$$

It is easily found that **K** must satisfy the relation

$$\widetilde{K}^2 = \frac{\omega^2}{c^2} + \frac{i\omega\mu_0\sigma_0}{1-i\omega\tau}, \quad \left[\widetilde{K} = \frac{\omega}{c}\widetilde{N}\right]. \quad \text{--- (2-1-21)}$$

In the condition of very low frequency, the formula is reduces to the approximate formula

$$\widetilde{K}^2 \approx i\omega\mu_0\sigma_0, \quad K \approx \sqrt{i\omega\mu_0\sigma_0} = (1+i)\sqrt{\omega\mu_0\sigma_0/2}; \quad \text{--- (2-1-22)}$$

In the low frequency case, the real and imaginary parts of **K** are equal.

(**K**=k+iα), $k \approx \alpha \approx \sqrt{\omega\mu_0\sigma_0/2}$. --- (2-1-23)

Similarly, the real and imaginary parts of **N** are equal too.

(**N**=n+iκ), $n \approx \kappa \approx \sqrt{\sigma_0/2\omega\varepsilon_0}$. --- (2-1-24)

Without the assumption, we drive the complex refraction index from the relation of **K**.

$$N^2 = 1 - \frac{\omega_p^2}{\omega^2 + i\omega\tau^{-1}}, \quad \text{plasma frequency: } \omega_p = \sqrt{\frac{Ne^2}{m\varepsilon_0}} = \sqrt{\frac{\mu_0\sigma_0 c^2}{\tau}} . \quad \text{--- (2-1-25)}$$

Drude Smith Model: [17]

While THz is widely used in Chemistry research and measurements of the conductivity of semiconductor, the flexibility Drude model have been invested in THz region. Better fits model are in the form of modified Lorentzians

$$\widetilde{\sigma}(\omega) = \frac{\sigma_0}{[1-(i\omega\tau)^{1-\alpha}]^\beta}, \quad \text{--- (2-1-26)}$$

where the exponents $1-\alpha$ and β are treated as disposable parameters. With $\alpha=0$ and $\beta=1$, we have the Drude result. With $\beta=1$ and α setting as variables is called the Cole-Cole(CC) model. With $\alpha=0$ and varying the value of β, it is called the Cole-Davidson(CD) model. Some well-fit results were published in the past literature, such as:

On doped Si, Grischkowsky et al. report success with CD model and in transient photoconductivity measurements on GaAs, Schmuttenmaer et al. report success with keeping both α and β as varying parameters.

The formula with Lorentzian form requires that the frequency dependent conductivity should have the maximum at the zero frequency and then fall off. Departure phenomena have been observed, and we have to concern with those materials in which $\sigma(\omega)$ displays a minimum at zero frequency and a transfer of oscillator strength to higher frequencies in the form of an impulse response.

Let us introduced a simple impulse response approach to the optical conductivity, we have the initial current decays exponentially to its equilibrium value with a relaxation time τ as the form

$$\frac{j(t)}{j(0)} = e^{(-\frac{t}{\tau})}, \quad \text{--- (2-1-27)}$$

and $\tilde{\sigma}(\omega) = \frac{Ne^2\tau}{m}\left(\frac{1}{1-i\omega\tau}\right);$ --- (2-1-28)

It is the form of Drude model. Then let us assume that an electron experiences collisions that are randomly distributed in time but with an average time interval τ between collision events. We have the resulting current response

$$\frac{j(t)}{j(0)} = e^{(-\frac{t}{\tau})}\left[1 + \sum_{n=1}^{\infty} c_n \cdot \frac{(\frac{t}{\tau})^n}{n!}\right],$$ --- (2-1-29)

And $\tilde{\sigma}(\omega) = \frac{Ne^2\tau}{m}\left(\frac{1}{1-i\omega\tau}\right)\left[1 + \sum_{n=1}^{\infty} \frac{c_n}{(1-i\omega\tau)^n}\right];$ --- (2-1-30)

This generalized Drude formula is called Drude Smith model following the name of the inventor, Smith. The coefficient c_n represents the fraction of the electron's original velocity that is retained after the n_{th} collision. In order to simplify our calculation, we assume that the persistence of velocity is retained for only one collision ($c_n=0$, for n>1). We have the current response

$$\frac{j(t)}{j(0)} = e^{(-\frac{t}{\tau})}\left[1 + \frac{ct}{\tau}\right],$$ --- (2-1-31)

and $\tilde{\sigma}(\omega) = \frac{Ne^2\tau}{m}\left(\frac{1}{1-i\omega\tau}\right)\left[1 + \frac{c}{1-i\omega\tau}\right];$ --- (2-1-32)

For elastic collisions, c would be <cosθ> where θ is the scattering angle. The most important character of c is described as followed: When c is a negative value, it implies a predominance of backscattering.

2-2　The Method of Measurement and Data Analysis

Thin Film Sample (Transmission Type THz-TDS)

Considering a thin film with a thickness below 150μm, the time delay of it will be smaller than 1ps which is the duration of THz pulse. We cannot distinguish the second reflection from the main pulse. Therefore we introduce the multi-beam interference in our analysis as that to extract the information from the THz waveform by Fourier transform method (time domain to frequency domain). And then, we take the refraction index of substrate as a constant value to simplify the analysis method. (In practical, we use low absorption and constant refraction index material in THz range.)

Theoretical transmission formula

$E_0(\omega)$ is the incident THz field, $E_{ref}(\omega)$ is the reference electric field gone through both the substrate (the thickness is "D") and a bunch of air with thickness "d", and $E_{sig}(\omega)$ is the signal electric field transmitted through both the thin film (the thickness is "d") and the substrate (the thickness is "D"). We could write down the reference and signal field in the form of E_0:

* $E_{ref}(\omega) = t_{13}t_{31}E_0(\omega)e^{i\frac{n_3\omega(d+D)}{c}}$； --- (2-2-1)

* $E_{sig}(\omega) = t_{31}E_{film}(\omega)e^{i\frac{n_3\omega D}{c}}$； --- (2-2-2)

With $E_{film}(\omega) = E_0(\omega)t_{12}t_{23}e^{i\frac{\tilde{n}_2\omega d}{c}} + E_0(\omega)t_{12}t_{23}r_{21}r_{23}e^{i\frac{3\tilde{n}_2\omega d}{c}} + E_0(\omega)t_{12}t_{23}r_{21}^2 r_{23}^2 e^{i\frac{5\tilde{n}_2\omega d}{c}} +$

$\cdots + E_0(\omega)t_{12}t_{23}r_{21}^q r_{23}^q e^{i\frac{(2q+1)\tilde{n}_2\omega d}{c}}$；

--- (2-2-3)
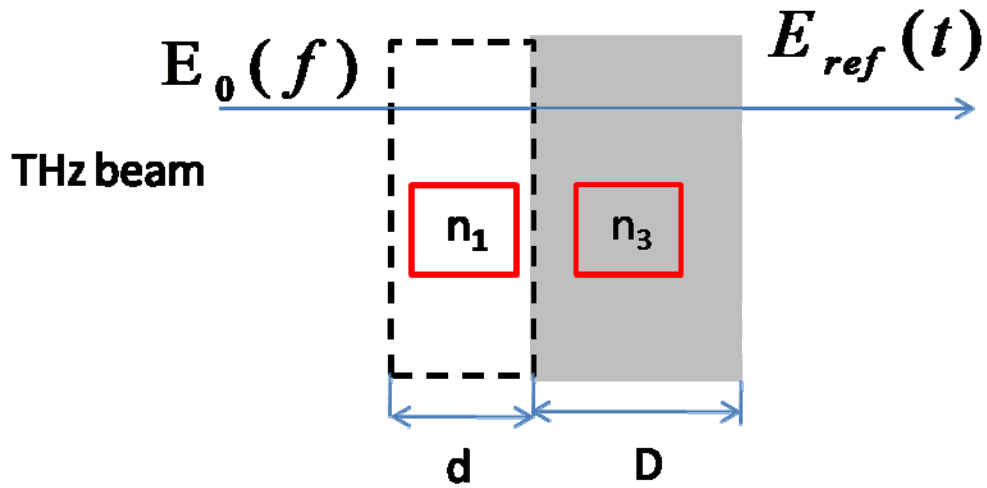
Fig. 2-2-1 The diagram of the reference
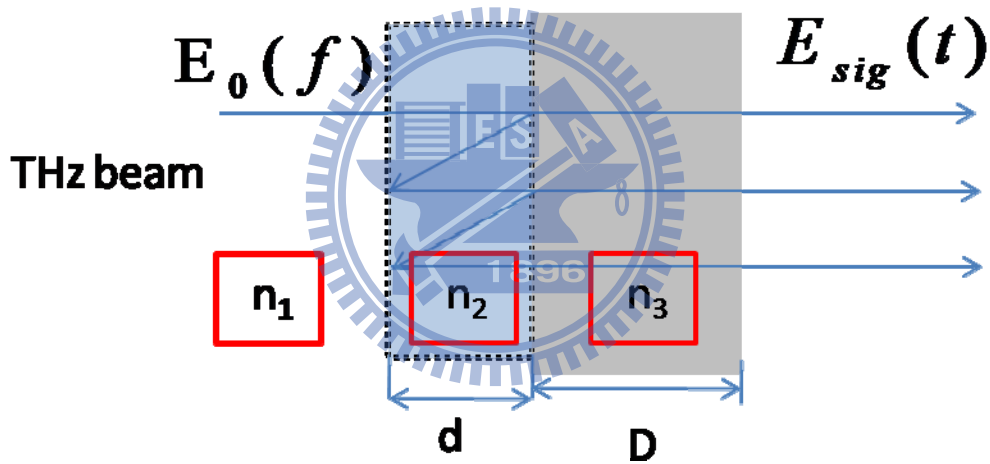
Fig. 2-2-2 The diagram of the sample

Fig. 2-2-1 and 2-2-2 are showing the basic diagrams of the light propagating

through the sample and the reference. The concept will be applied to the THz-TDS

analysis with gathering both the reference and signal data.

Where q is the number of multiple reflections, and t_{12}, t_{13}, t_{31}, t_{23}, r_{21}, and r_{23} are Fresnel amplitude transmission and reflection coefficients in the condition of normal incidence which can be expressed by

$$t_{ij} = \frac{2n_i}{n_i + n_j}, \quad r_{ij} = \frac{n_j - n_i}{n_i + n_j}; \quad \text{---} \ (2\text{-}2\text{-}4)$$

By assuming the number of reflection is infinite ($q \rightarrow \infty$), $E_{film}(\omega)$ could be simplified as

$$E_{film} = E_0(\omega) \frac{t_{12}t_{23}e^{i\frac{\tilde{n}_2\omega d}{c}}}{1 - r_{21}r_{23}e^{i\frac{2\tilde{n}_2\omega d}{c}}}; \quad \text{---} \ (2\text{-}2\text{-}5)$$

From the equation 2-2-1 and 2-2-2 by insert 2-2-5 into them, the theoretical complex transmittance can be given by

$$\tilde{t}_{the}(\omega) = \frac{\tilde{E}_{sig}(\omega)}{\tilde{E}_{ref}(\omega)} = \frac{t_{12}t_{23}e^{i\frac{(\tilde{n}_2 - 1)\omega d}{c}}}{t_{13}(1 - r_{21}r_{23}e^{2i\frac{\tilde{n}_2\omega d}{c}})}; \quad \text{---} \ (2\text{-}2\text{-}6)$$

With

$$t_{12} = \frac{2n_1}{n_1 + \tilde{n}_2}, \quad t_{23} = \frac{2\tilde{n}_2}{\tilde{n}_2 + n_3}, \quad t_{13} = \frac{2n_1}{n_1 + n_3}, \quad r_{21} = \frac{n_1 - \tilde{n}_2}{n_1 + \tilde{n}_2}, \quad r_{23} = \frac{n3 - \tilde{n}_2}{n3 + \tilde{n}_2}; \quad \text{---} \ (2\text{-}2\text{-}7)$$

The contents mentioned above where n_1 is the refraction index of the air, $\tilde{n}_2$ is the complex refraction index of the thin film, and n_3 is the refraction index of the substrate.

Refraction index extraction

Experimental data is collected from transmission type THz-TDS system with PC antenna as emitter and receiver. By means of the Fourier transform, the original time domain data is to be the frequency domain data. Therefore we have the experimental amplitude transmission in frequency domain by dividing the two spectrums, here we

given it by $\tilde{t}_{\exp}(\omega, n_2, \kappa_2)$.

In order to extract the parameters of the experimental data, we defined error function as below:

$$\left| \tilde{t}_{\exp}(\omega_i, n_2, \kappa_2) - \tilde{t}_{the}(\omega_i, n_2, \kappa_2) \right| = Error(\omega_i, n_2, \kappa_2);$$

First, given a periodic set of n_2 and κ_2, we set { n_2, 0, 200, 0.1 }, { κ_2, 0, 200, 0.1 }. (It means that an interval from 0 to 200 with spacing 0.1.) Then we can get a 2D-matrics of various n_2 and κ_2 at each ω_i. With the sorting program, we find out the local minimum of the 2D sets. Gathering all of the local minimums at each ω_i, we make a new set which is the refraction index extracting from the experimental data.
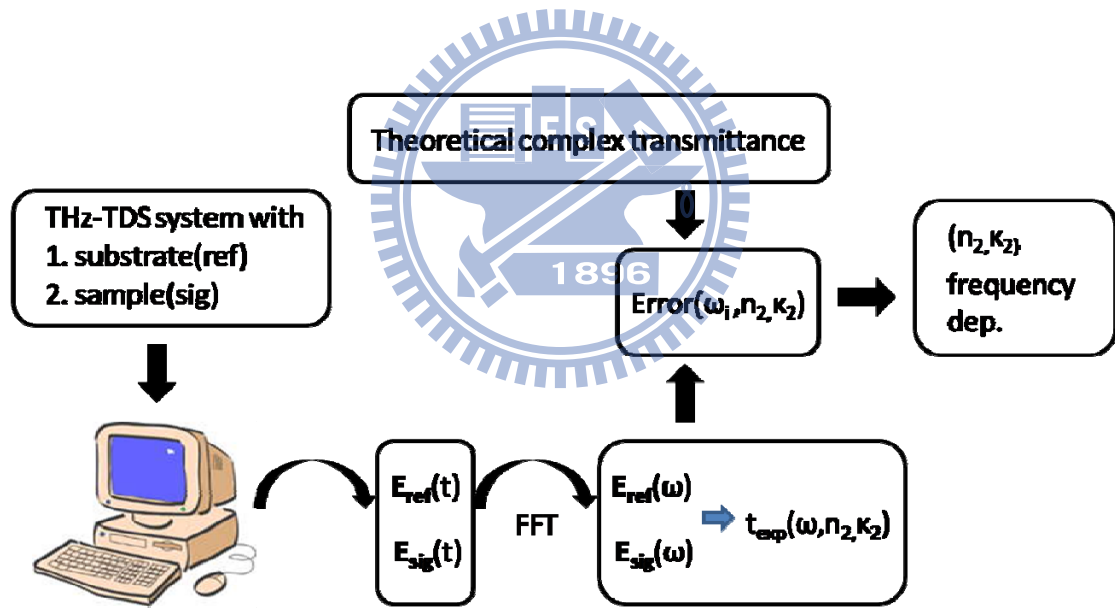
Fig.2-2-3 The flow chart of the n κ value extraction

Figure 2-2-3 demonstrates the flow chart of extracting the refractive index of the sample. First, we have the time domain waveforms, reference and signal, from the THz-TDS system. With the fast Fourier transform, we have the frequency domain spectrum. Then, we could get the experimental transmittance. Following, to calculate the fitting result, we define the error function with theoretical transmittance and the

experimental data. By calculating from computer program, we could extract the frequency dependent refractive index.

Optical conductivity

From above calculations, we have the complex refractive index, and we can use it to obtain the complex conductivity of a conductor. First, we start from the Maxwell equation assuming a simple conducting medium with a flowing current, **J**=σ**E**, and the formula can be expressed by:

$$\nabla \times \vec{H} = \vec{J} + \frac{\partial \vec{D}}{\partial t} = \vec{J} - i\omega\varepsilon_0\varepsilon_\infty \vec{E}$$

$$= -i\omega\varepsilon_0[\varepsilon_\infty - \frac{\tilde{\sigma}}{i\omega\varepsilon_0}]\vec{E} = -i\omega\varepsilon_0\varepsilon_\infty\vec{E},$$

$$\Rightarrow \tilde{\varepsilon} = \varepsilon_\infty + i\frac{\tilde{\sigma}}{\omega\varepsilon_0};$$

--- (2-2-8)
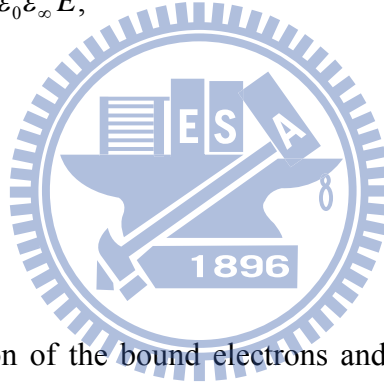
where ε_∞ is the contribution of the bound electrons and ε is the effective dielectric constant. We can have ε from the refractive index via the relation of $\varepsilon=(\varepsilon_r+i\varepsilon_i)=(n+i\kappa)^2$ and therefore the complex conductivity can be obtained from Eq.

$$\tilde{\sigma}(\omega) = (\sigma_r + i\sigma_i) = i\omega\varepsilon_0(\varepsilon_\infty - \tilde{\varepsilon}),$$
$$\sigma_r = \omega\varepsilon_0\varepsilon_i,$$
$$\sigma_i = \omega\varepsilon_0(\varepsilon_\infty - \varepsilon_r);$$

--- (2-2-9)

The conduction of electrons in simple metals can be describe by a classical simple Drude model [18] which treat the free carriers in a solid as classical point charges

subject to random collisions denoted as

$$\tilde{\sigma}(\omega) = \sigma_r + i\sigma_i = \frac{\varepsilon_0 \omega_p^2 \tau}{1 - i\omega\tau},$$

$$\sigma_r(\omega) = \frac{\varepsilon_0 \omega_p^2 \tau}{1 + \omega^2\tau^2},$$

$$\sigma_i(\omega) = \omega \frac{\varepsilon_0 \omega_p^2 \tau^2}{1 + \omega^2\tau^2};$$

--- (2-2-10)

The plasma frequency is defined by $\omega_p^2 = Ne^2/(\varepsilon m^*)$ where N is carrier concentration, e is the electronic charge and m^* is the effective carrier mass, and τ is the carrier relaxation time. The DC conductivity is given by $\sigma_{DC} = eN\mu$, where $\mu = e\tau/m^*$ is the carrier mobility. The simple Drude model indicates that the velocity of carriers is damped with a time constant τ and is randomized following each collision event. The conduction properties of many semiconductors in the terahertz region have been justified to follow the simple Drude model, but some nanostructured materials show deviations from it. Recently, Smith proposed a modified Drude model, which can explain the deviations from the simple Drude model for the nanostuctured materials, particularly the negative values of imaginary part of conductivity. The complex conductivity in the Drude-Smith model [17] is given by

$$\tilde{\sigma}(\omega) = \frac{Ne^2\tau}{m} \left(\frac{1}{1 - i\omega\tau}\right)\left[1 + \frac{c}{1 - i\omega\tau}\right] = \frac{\varepsilon_0 \omega_p^2 \tau}{1 - i\omega\tau}\left[1 + \frac{c}{1 - i\omega\tau}\right]; \quad \text{--- (2-2-11)}$$

where c is a parameter describing fraction of the electron's original velocity after scattering and vary between -1 and 0. In the simple Drude model, the momentum of carrier is randomized after each scattering event, but in the Drude-Smith model,

24

carriers retain a fraction, c, of their initial velocity. In particular, $c = 0$ corresponds to the simple Drude conductivity and $c = -1$ means that carrier undergoes complete backscattering. The Drude-Smith model predicts a DC conductivity of $\sigma = eN\mu(1+c)$ and thus the reduced macroscopic DC mobility is given by $\mu_m = (1+c)\mu$. [17]
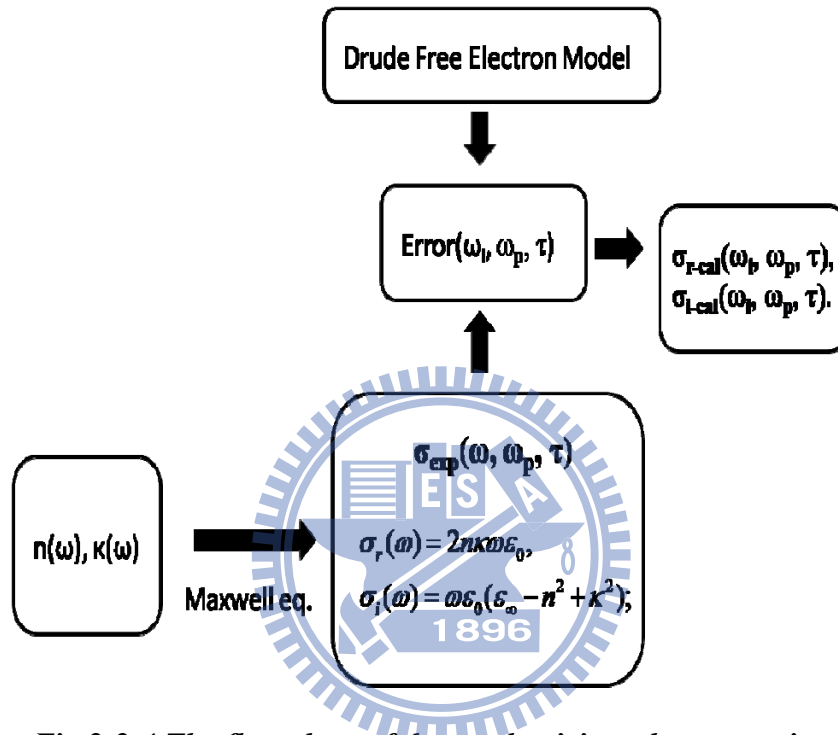
Fig.2-2-4 The flow chart of the conductivity value extraction

Figure 2-2-4 demonstrates the flow chart of the conductivity value extraction. It follows the steps as below. To get the experimental conductivity from the refractive index, we use the relations between the refractive index to the permittivity and the conductivity to the permittivity. The relations are derived from Maxwell equations. And then, we introduce Drude free electron model into the fitting process. With the experimental data and theoretical formula, we also define an error function to extract our parameters, ω_p and τ.

2-3 Effective Medium Approximation:

If the body is neutral, the contribution to the average field may be expressed in terms of the sum of the fields of atomic dipoles. We define the average electric field **E** (r_0) as the average field over the volume of the crystal cell that contains the lattice point r_0:

$$\overline{E}(r_0) = \frac{1}{V_c} \int dV \cdot \vec{e}(\vec{r}), \quad \text{--- (2-3-1)}$$

where **e(r)** is the microscopic electric field at the point **r**. V_c is the total volume of the body. We called **E** the macroscopic electric field.

Depolarization Field: [19]

The geometry in many of our problems is such that the polarization is uniform within the body, and then the only contributions to the macroscopic field are from E_0 and E_1:

$$\overline{E} = \overline{E}_0 + \overline{E}_1; \quad \text{--- (2-3-2)}$$

Here **E**$_0$ is the applied field and **E**$_1$ is the field due to the uniform polarization. The field **E**$_1$ is called the depolarization field, for within the body it tends to oppose the applied **E**$_0$ as in Fig. 2-3-1.
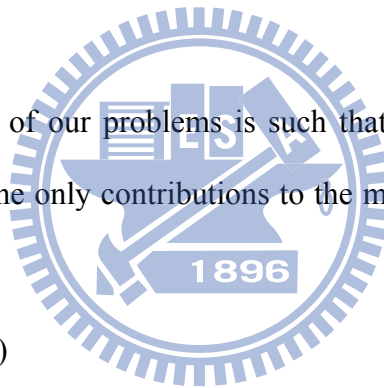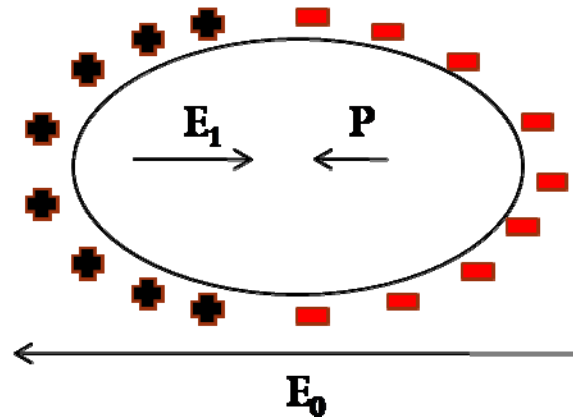
Fig.2-3-1 Depolarization field E₁ tends to oppose the applied field E₀.

If P_x, P_y, P_z are the components of the polarization **P** referred to the principal axes of an ellipsoid, then the components of the depolarization field are written

(CGS) $E_{1x} = -N_x P_x$; $E1y = -N_y P_y$; $E1z = -N_z P_z$; --- (2-3-3)

Nx, Ny, Nz are the depolarization factors and their values depend on the ratios of the principal axes of the ellipsoid.

Table 2-3-1 the depolarization factors for the body with different shapes

Shape	Axis	N(CGS)	N(SI)
Sphere	any	$4\pi/3$	1/3
Thin slab	normal	4π	1
Thin slab	in plane	0	0
Long circular cylinder	longitudinal	0	0
Long circular cylinder	transverse	2π	1/2

Local Electrical Field: [19]

The value of the local electric field that acts at the site of an atom is significantly different from the value of the macroscopic electric field. Now we consider the field

27

that acts on the atom at the center of the sphere. We write

$E_{local} = E_0 + E_1 + E_2 + E_3$. --- (2-3-4)

Here

E_0 = filed produced by fixed charges external to the body;

E_1 = depolarization field, from a surface charge density $\mathbf{n} \cdot \mathbf{P}$ on the outer surface of the specimen;

E_2 = Lorentz cavity field: field from polarization charges on inside of a spherical cavity cut out of the specimen with the reference atom as center.

E_3 = field of atoms inside cavity.
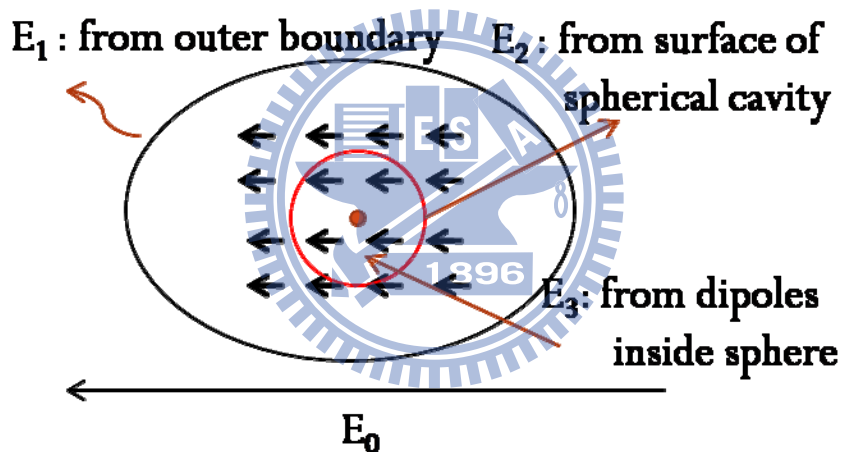
Fig.2-3-2 Electric fields act on the center of the ellipsoid on the site of an atom.

The contribution $E_1 + E_2 + E_3$ to the local field is the total field at one atom caused by the dipole moments of all the other atoms in the specimen:

$$\vec{E}_1 + \vec{E}_2 + \vec{E}_3 = \sum_i \frac{3(p_i \bullet r_i)r_i - r_i^2 p_i}{r_i^5}, \quad \text{(CGS)} \quad \text{--- (2-3-5)}$$

The total local field at a cubic site is

$$\vec{E}_{local} = \vec{E}_0 + \vec{E}_1 + \frac{4\pi}{3}\vec{P} = \vec{E} + \frac{4\pi}{3}\vec{P}; \quad \text{(CGS) --- (2-3-6)}$$

This is the Lorentz relation: the field acting at an atom in a cubic site is the

macroscopic field **E** of equation 2-3-2 plus 4π**P**/3 from the polarization of the other atoms in the specimen where the Lorentz cavity is considering as the spherical shape.

$$\vec{E}_2 = \int_0^\pi (a^{-2})(2\pi a \cdot \sin\theta)(a \cdot d\theta)(\vec{P} \cdot \cos\theta)(\cos\theta) = \frac{4\pi}{3}\vec{P}; \quad \text{(CGS) --- (2-3-7)}$$
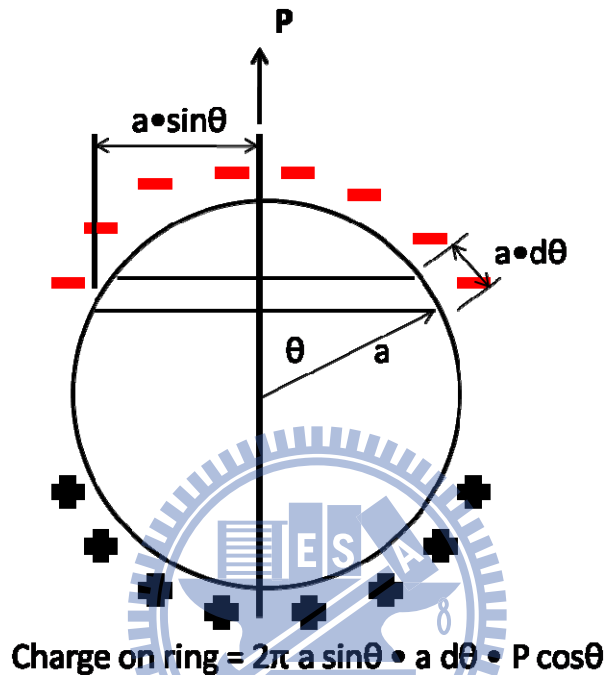
Fig.2-3-3 Calculation of the field in a spherical cavity in a uniformly polarized medium.

Clausius-Mossotti relation: [19]

The dielectric constant ε of an isotropic or cubic medium relative to vacuum is defined in terms of the macroscopic field E:

$$\varepsilon \equiv \frac{E + 4\pi P}{E} = 1 + 4\pi\chi; \quad \text{(CGS) --- (2-3-8)}$$

The susceptibility in equation (2-3-7) is related to the dielectric constant by

$$\chi = \frac{P}{E} = \frac{\varepsilon - 1}{4\pi}. \quad \text{(CGS) --- (2-3-9)}$$

29

The polarizability α of an atom is defined in terms of the local electric field at the atom:

$p = \alpha \cdot E_{local}$,   --- (2-3-10) where p is the dipole moment. The polarization of a crystal may be expressed approximately as the product of the polarizabilities of the atoms times the local electric field:

$$\vec{P} = \sum_j N_j p_j = \sum_j N_j \alpha_j E_{local}(j); \quad (CGS) --- (2-3-11)$$

where N_j is the concentration and α_j is the polarizability of atoms j, and E_{local} is the local field at atom sites j. With Lorentz relation, then

$$P = (\sum_j N_j \alpha_j)(E + \frac{4\pi}{3}P); \quad (CGS) --- (2-3-12)$$

By solving equation 2-3-11, we find the susceptibility

$$\chi = \frac{P}{E} = \frac{\sum_j N_j \alpha_j}{1 - \frac{4\pi}{3}\sum_j N_j \alpha_j}; \quad (CGS) --- (2-3-13)$$

By definition $\varepsilon = 1 + 4\pi\chi$ in equation 2-3-7, we may rearrange 2-3-12 to obtain

$$\frac{\varepsilon - 1}{\varepsilon + 2} = \frac{4\pi}{3}\sum_j N_j \alpha_j; \quad (CGS) --- (2-3-14)$$

This relation between the dielectric constant and the electric polarizability is called the Clausius-Mossotti relation.

Heterogeneous Dielectric and Effective-Midium Theory: [20]

We consider the multiphase mixtures contained more than two homogeneous material constituents.

Therefore the total polarization density from each quest phase contributes one such term to a sum of many is described in equation 2-3-11.

$$\overline{P} = \sum_{j=1}^{K} N_j p_j, \qquad \text{(CGS)} \text{ --- (2-3-15)}$$

where N_j is the number density of the jth inclusion phase, and p_j is the dipole moment of a single inclusion of that phase. Here the number of different materials forming the mixture is K+1 because the environment material is not counted in the sum. With the Clausius-Mossotti relation, the final result for the effective permittivity is

$$\frac{\varepsilon_{eff} - 1}{\varepsilon_{eff} + 2} = \sum_{j}^{K} \frac{4\pi}{3} N_j \alpha_j = \sum_{j}^{K} f_j \frac{\varepsilon_j - 1}{\varepsilon_j + 2}; \qquad \text{(CGS)} \text{ --- (2-3-16)}$$

where f_j is the volume fraction of the inclusions of the jth phase in the mixture, α_j is the polarizability of such a sphere, and ε_j is its permittivity. As the result of the definition for f_j,

$$\sum_{j}^{K} f_j = 1; \quad (2-3-17)$$

The equation 2-3-16 is obviously using at two phase mixtures to do our analysis.
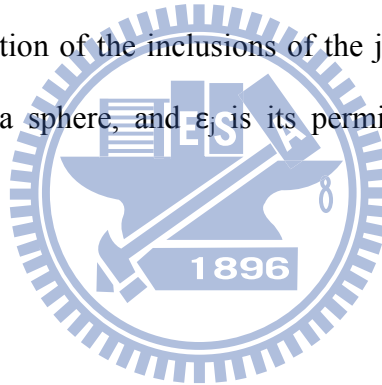
Chapter 3 : ITO thin film characterization

3-1 Characters of Samples

ITO Thin Film (with O$_2$ flux) shown in Fig. 3-1-1 to 3-1-3
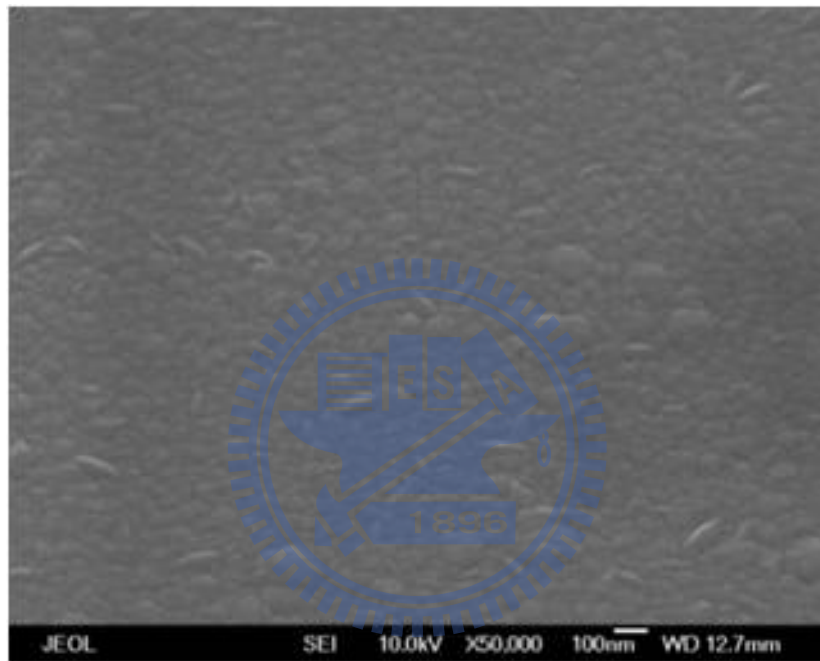
Fig. 3-1-1 Film with thickness 961.6(nm)

The Fig.3-1-1 to 3-1-3 show the top views of our ITO film samples. The magnification is ×50,000. The pictures with a scale 100nm make us find out the grain size of each sample. Therefore, we have the grain size, 30nm, 20nm, 10nm for the sample with thickness, 961.6nm, 483.0nm, 188.9nm, respectively.
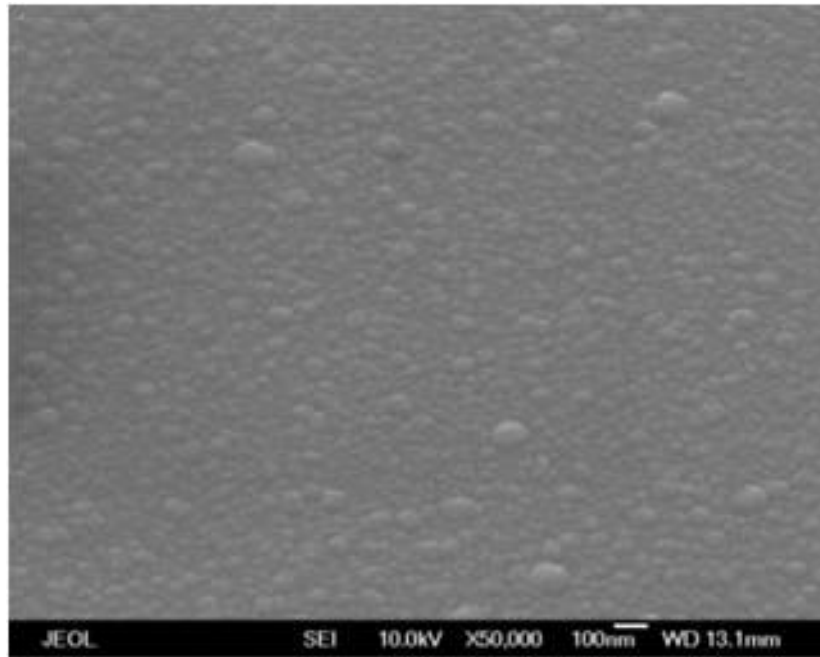
Fig. 3-1-2 Film with thickness 483.0(nm)
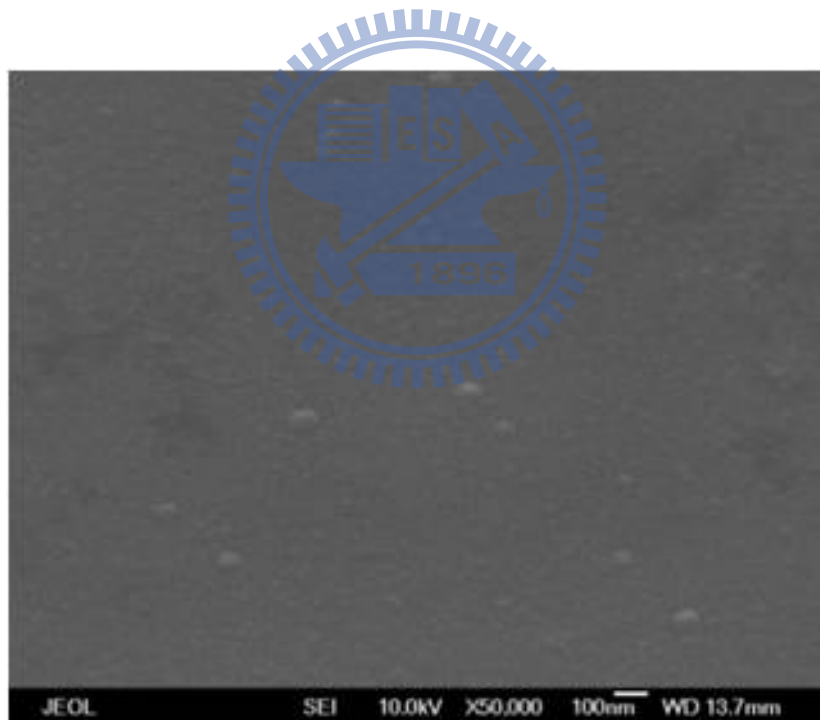
Fig. 3-1-3 Film with thickness 188.9(nm)

In the SEM of ITO thin film, the grain size increasing is proportion to the film thickness. The value of the grain sizes are around several nm (30 nm to few nm). In the literature, the electron mean free path is below 5nm. [21] It means that the

dominate scattering mechanism of optical measurement is the same as the Hall measurement. In conclusion, we shall get a set of data by optical system being close to the hall measurement.

The cross diagram of ITO film with O_2 flux has the geometry structure as below: in Fig.3-1-4
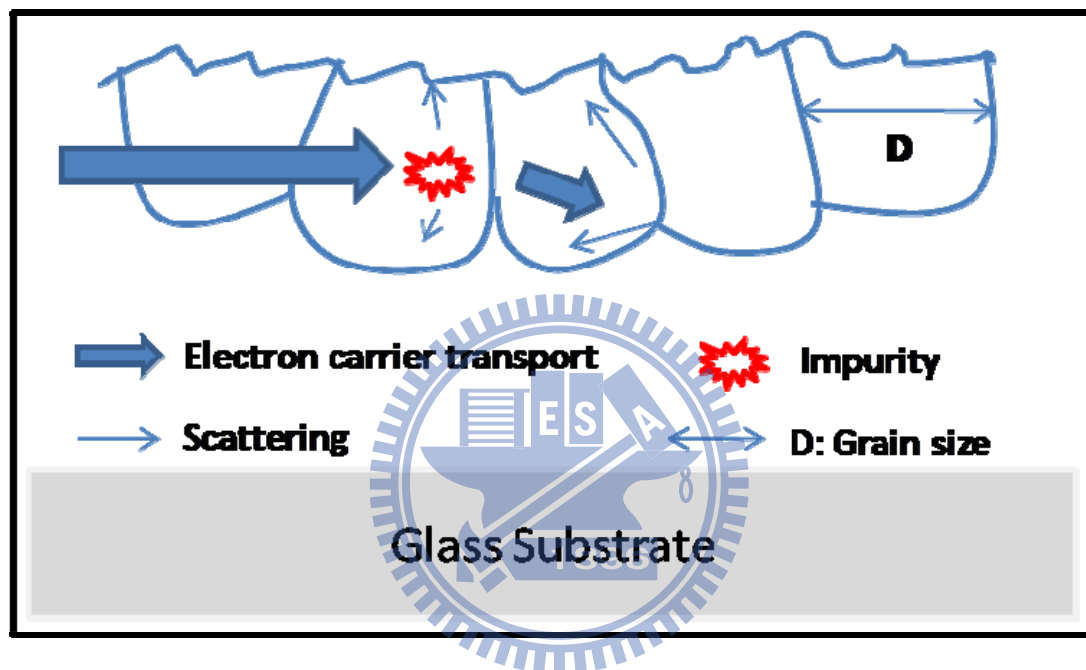
Fig.3-1-4 The electron scattering at the grain boundary and the ionized impurity
[22]

There are many sources of electron scattering may influence the optical and electrical properties. The effects can separate between electron-defect scattering (i.e. grain boundaries and external surface, neutral and ionized point defects, dislocations, precipitations, and clusters), electron-lattice scattering (i.e. local deformation potentials), and electric-electron scattering. Original Drude model theory, without the damping term, is not sufficient for a quantitative model of the free electron properties in our sample. That is so because the damping term γ was introduced to our model. [21]

Optical Spectroscopy of ITO Thin Film

The spectra of transmission type and reflection type spectrometer can distinguish the ITO film in different growth parameters, such as thickness [22], wt% of the target [23], and the flux of gas [24] et al.

In our case, all the conditions are fixed except the thickness of ITO films which are 961.6nm, 483.0nm, and 188.9nm. The thickness of ITO films are measured by "n & k-1500" at the center of our sample. The commercial "n & k 1500" are provided by NDL. The Fig.3-1-5 shows the plasma edge is increasing as the film thickness increasing. Around the plasma frequency, there is an important signature that is plasma edge where has the strong increase of absorption or reflection in the spectrum for transmission type or reflection type respectively. As the complex permittivity is describe by $\varepsilon=\varepsilon_r+i\varepsilon_i$, the plasma frequency Ω_p is defined by $\varepsilon_r(\Omega_p)=0$.

We have to notice that Ω_p is not equal to ω_p, the Drude plasma frequency, mentioned in chapter 2. They have the relationship

$$\Omega_p = \sqrt{\frac{\omega_p^2}{\varepsilon_\infty} - \frac{1}{\tau^2}}, \quad \text{--- (3-1-1) [22]}$$

where τ is the scattering time and ε_∞ is the relative permittivity at high frequency range. In conclusion, the value of Ω_p will smaller than the value ω_p calculated from Drude model.

Otherwise, we also can find out the energy band gap of the ITO is around 400nm ~ 3.1eV.
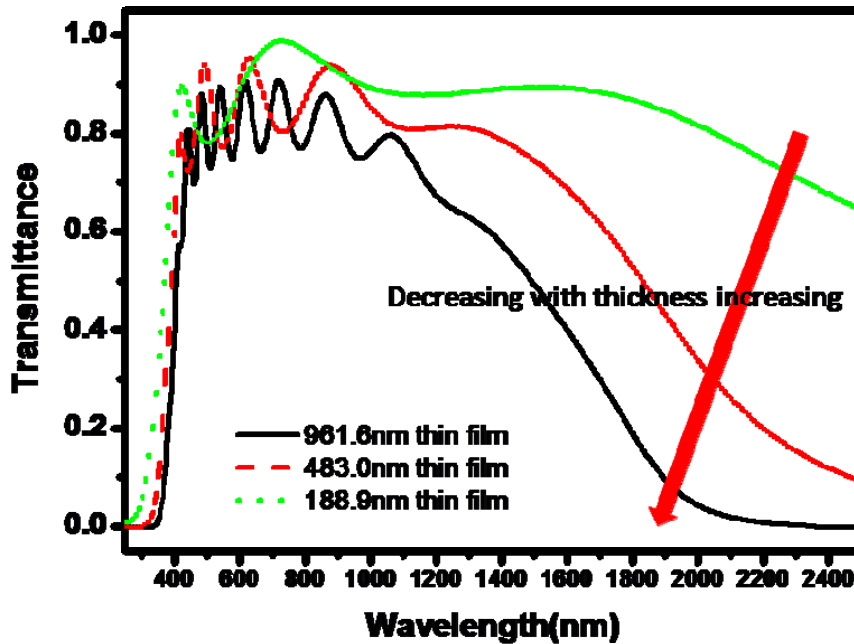
Fig.3-1-5 Spectra of JASCO: V-670 spectrometer (transmission type) for thin ITO films of the different thickness: 961.6nm, 483.0nm, and 188.9nm

In the Fig.3-1-5, we find out that as the thickness increasing the plasma edges are decreasing in the view of wavelength. The plasma edges are pointed by the arrow. [22]

Reflection Type Far Infrared Spectroscopy (R-FTIR)

The FTIR spectra were recorded using "Bomen da8.3" spectrometer by Instrument Center at National Tsing Hua University. The angle of incidence is 18° related to the sample normal. A ratio of the single beam spectra of ITO films to a single beam spectrum of a planar gold mirror was performed to obtain the reflectance spectra of ITO films with a 6mm hole to confine the detection range. The whole spectra cover from 0.6μm to 71.6μm (i.e. 15000cm^{-1} to 140cm^{-1}).

Fig.3-1-6 FTIR of ITO film at short wavelength range with lower reflection part

Fig.3-1-7 FTIR of ITO film at long wavelength range with higher reflection part

(The horizontal axis is in log scale.)

Similarly, we also can find out that the plasma edges are decreasing with the increasing of thickness (in the view of plasma wavelength). At the high frequency part, i.e. short wavelength part here, there are some vibrations which are the phenomena near the plasma edge. They also show strong thickness dependant that the t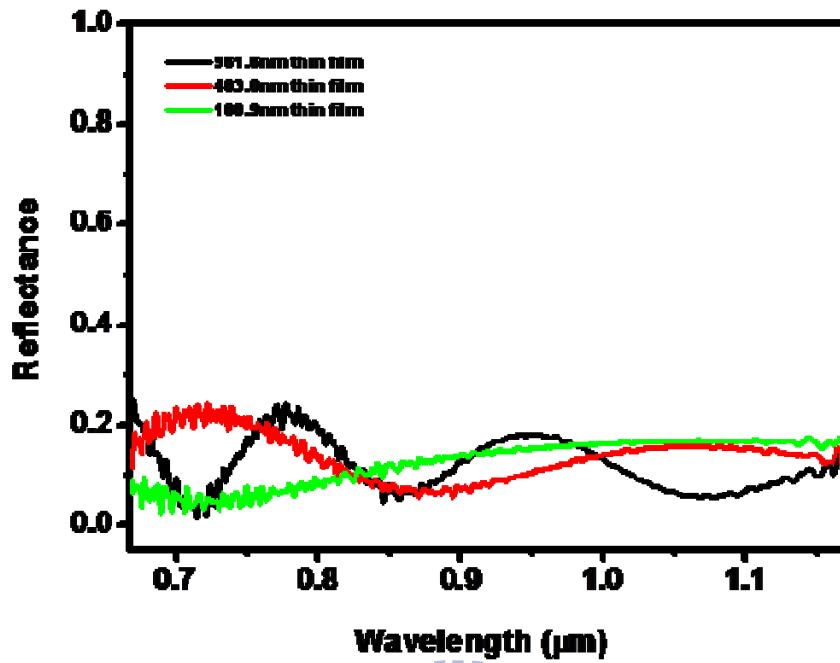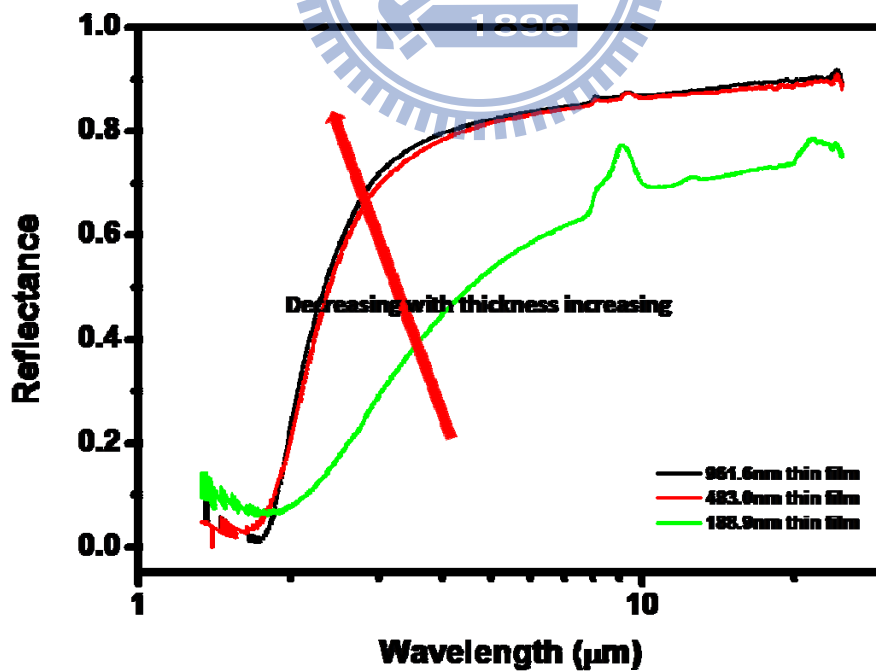hicker one has a high frequency variation in the part of short length edge, contrarily, for the thinner one. Both the transmission spectra and the reflection spectra have found the phenomena.

Hall Measurement

To act as a good electrode for solar cell, it should have both the good transparent property in solar range and low sheet resistivity (<10 Ω). [13] We have to deal our samples with optical measurement and electric measurement. The Hall measurement is used to get the electrical properties of the thin film samples. The model of the machine is "Ecopia HMS-3000".
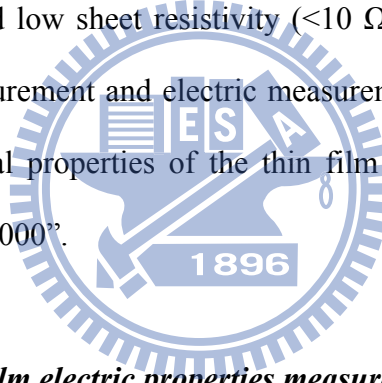
Table 3-1-1 ITO thin film electric properties measured by Hall measurement

By Hall (film on fused silica)	N (cm^{-3})	μ $(cm^2V^{-1}s^{-1})$	σ_0 $(\Omega^{-1}cm^{-1})$	ρ $(\Omega \cdot cm)$
188.9 (nm)	-2.5×10^{20}	38.4	1557	6×10^{-4}
483.0 (nm)	-3.4×10^{20}	38.0	2045	5×10^{-4}
961.6 (nm)	-4.1×10^{20}	34.3	2250	4×10^{-4}

In the above table, carrier concentration is N, mobility is labeled by μ, DC conductivity is denoted by σ_0, and resistivity is given a symbol as ρ. With the Hall

measurement, we find out some characters of the thin film samples. The carrier concentrations and the DC conductivity increase as the thickness becoming larger. The Hall mobility of the thin films is close to each other.

Table 3-1-2 The sheet resistivity of Hall measurement compared with 4-point probe measurement

Hall v.s. 4-point probe (film on fused silica)	Sheet R ($\Omega/\square$)-Hall	Sheet R ($\Omega/\square$)-NDL
188.9 (nm)	34.03	36.05
483.0 (nm)	10.1	10.48
961.6 (nm)	4.62	4.62

The sheet resistivity of Hall is closely to the 4-point probe method for the ITO film at each thickness. It is a recheck. With the growth of the sample thickness, the sheet resistivity becomes smaller. ITO thin film with thickness, 961.6nm, has the lowest sheet resistivity bellowing $10\,\Omega/\square$. It means that it turns to be the crystalline structure. It will be proved in the spectrum of X-ray diffraction.

3-2 Reflection Type FTIR using Drude Model fitting

ITO thin films have been widely studied in the optoelectronic industry because they combine unique transparent and conducting properties. The optical research of ITO in FTIR is also well studied with Drude free electron model by different assumption details. There are some examples:

In earlier 1980s, they dealt the problem with simple optical reflection assumption, A=1-R-T, to extract $\varepsilon(\omega)$. A is the power absorption, R is the power reflection, and T

is the power transmission. [25] The group, D. Mergel et al, did it also with simple optical assumption. Otherwise, they modified the dielectric model to have more parameters as variables to well fit the curve of the ITO film FTIR spectrum. [26] FTIR spectra of ITO film with different angle incidence were fitted with two-phase Fresnel equations and three-phase Fresnel equations for Reflectance by the group, H. Scott et al. [27] Therefore, using the Drude model to extract the information of ITO thin film is a well known method.

Fitting Model and Reflectance FTIR Spectroscopy

The spectra of ITO film determined by NDL using a Bruker IFS66v/S spectrometer are used to do the following analysis. The spectra were obtained with incident angle 11° and a hole 7mm on the sample mount. Gold mirror was used as reference spectrum in the measurement. With a spectrum range, 400 cm^{-1} to 7500 cm^{-1}, reflection type FTIR of ITO films were recorded.
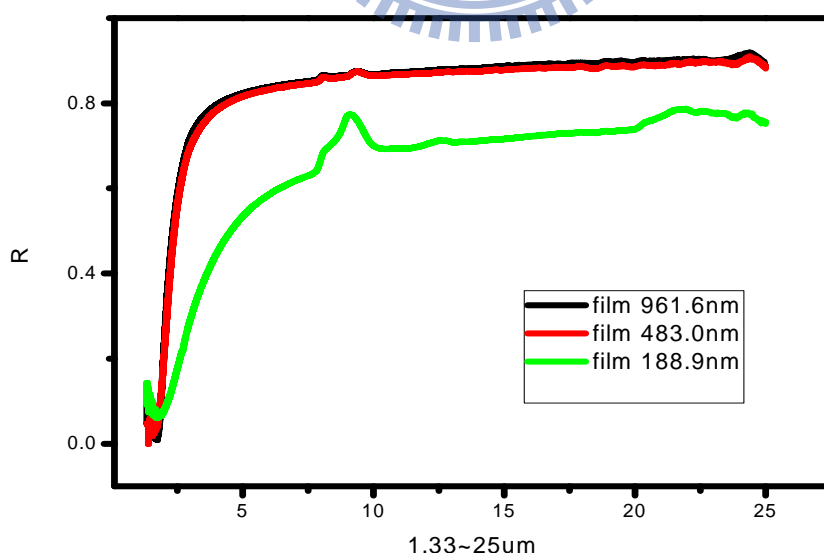

Fig.3-2-1 Spectra of ITO film by reflection type FTIR (400 cm^{-1} to 7500 cm^{-1})

The peaks around 25 μm and 10 μm are the phonon absorption. [21] With the thickness growth up, the reflection peaks will become smaller or undetermined. It could be modeling by introducing the damped Lorentz oscillators in infra-red range. But in our modeling, we neglect the phonon part to do the fitting process.

How to model the curvature of ITO FTIR spectra? The Drude free electron model is used to fit ITO film spectra.

$$\varepsilon(\omega) = \varepsilon_\infty - \omega_p{}^2 \frac{1}{\omega^2 + i\dfrac{\omega}{\tau}};$$

where ε_∞ is the high frequency dielectric constant, ω_p is the Drude plasma frequency, ω is the frequency, and τ is the electron scattering time.

The plasma frequency is defined by $\omega_p{}^2 = Ne^2/m\varepsilon_0$, where N is the carrier concentration. With the three-phase Fresnel equations for reflectance, we have

$$r_p = \frac{r_{p12} + r_{p23}e^{2i\delta}}{1 + r_{p12}r_{p23}e^{2i\delta}}, \delta = 2\pi\frac{d}{\lambda}\widetilde{N}\cos\Theta.$$ The subscript "p" means that in p – polarization

and the basic diagram of the sample is "1/2/3 to air/ITO/glass (FS)". δ is the path difference and $\widetilde{N}$ is the complex refraction index of ITO film.

With the two assumptions above, we can get the theoretical expression of reflection for ITO film. The diagram of flow chart as shown in next page: Fig.3-2-2
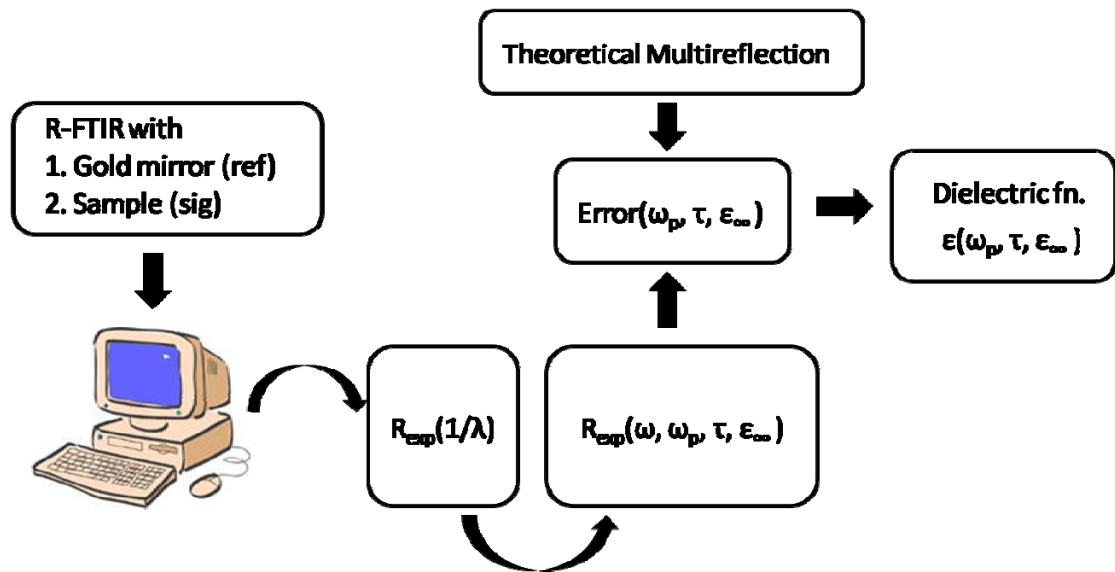
Fig.3-2-2 It shows how to get the plasma frequency, and carrier scattering time from FTIR spectra.

In the Fig.3-2-2, it is the flow chart of FTIR reflectance spectrum fitting. Bruker IFS66v/S spectrometer was used to get the spectrum with the x-axis is the wave number. Then we have to transverse the data to angular frequency dependent. With the theoretical formula and the experimental results, we can define a error function in our fitting process to extract the parameters, ω_p and τ, the plasma frequency and the carrier scattering time.

ITO FILM (FS) : 188.9nm
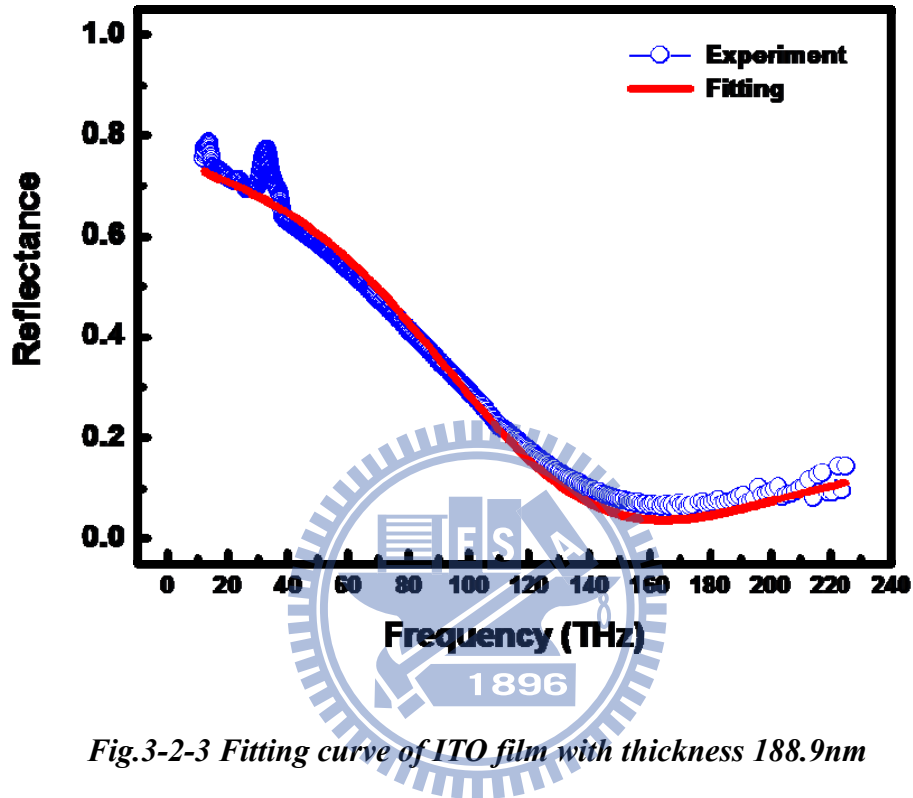
Fig.3-2-3 Fitting curve of ITO film with thickness 188.9nm

Table3-2-1 Fixed parameters

ε_∞	n_{FS}
4	1.4

Table3-2-2 Fitting parameters of ITO film 188.9nm

ω_p(rad.THz)	τ(fs)	μ(cm^2/Vs)	N(cm^{-3})
1600	6.8	34.2	2.8×10^{20}
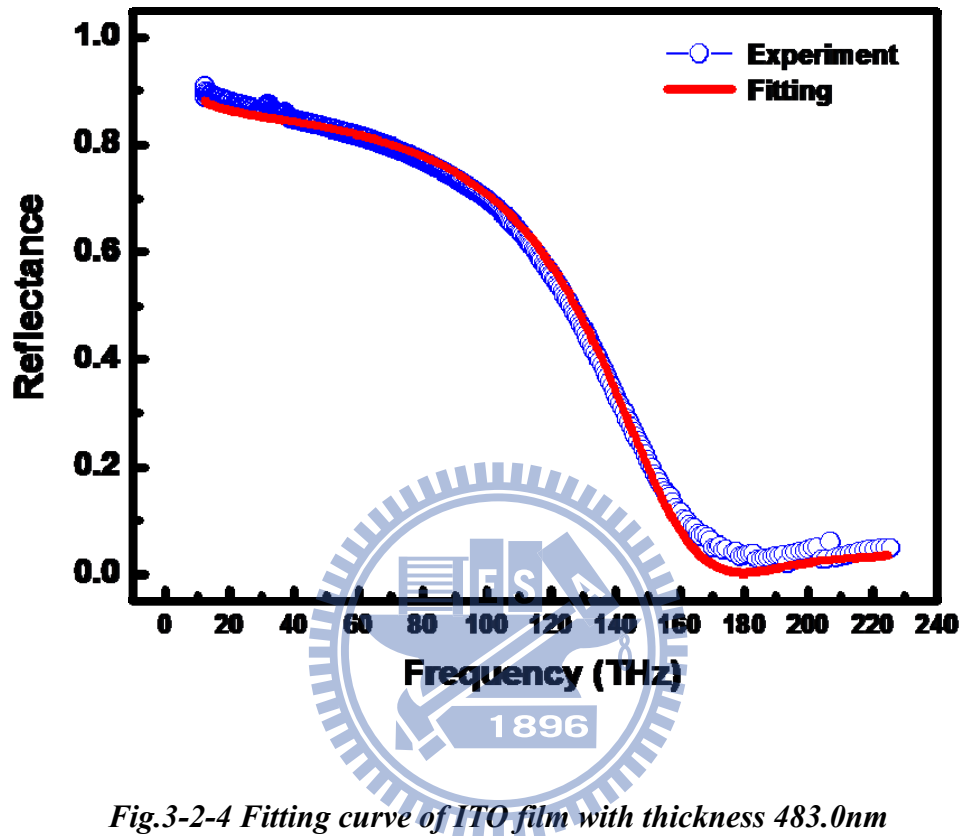
Fig.3-2-4 Fitting curve of ITO film with thickness 483.0nm

Table3-2-1 Fixed parameters

ε_∞	n_{FS}
4	1.4

Table3-2-3 Fitting parameters of ITO film 188.9nm

ω_p(rad.THz)	τ(fs)	μ(cm^2/Vs)	N(cm^{-3})
1860	6.7	33.7	3.8×10^{20}

ITO FILM (FS) : 961.6nm
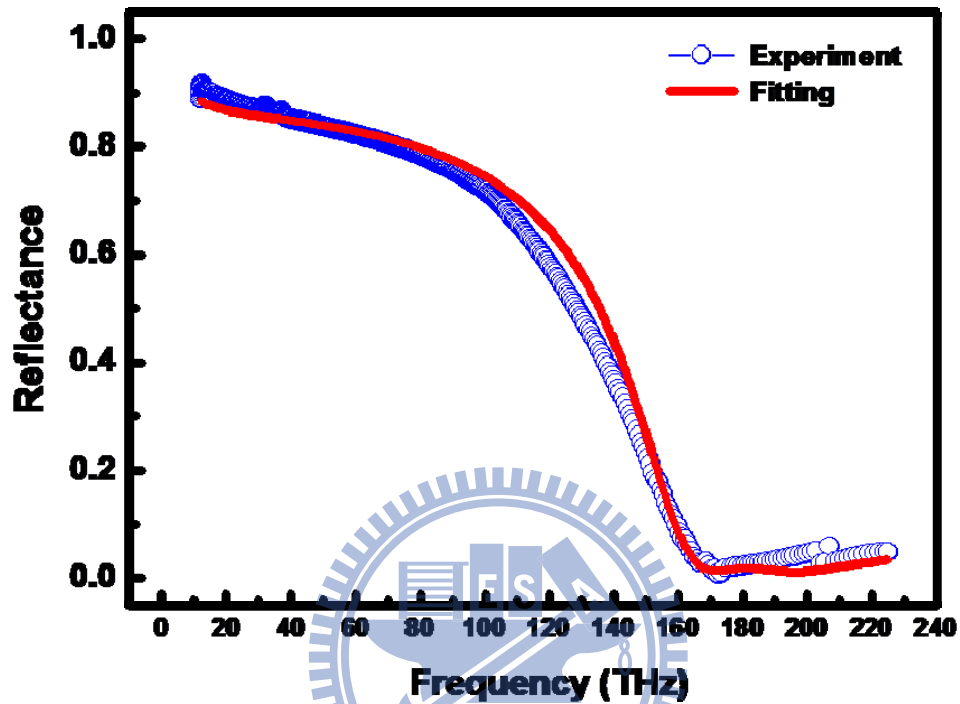
Fig.3-2-5 Fitting curve of ITO film with thickness 961.6nm

Table3-2-1 Fixed parameters

ε_∞	n_{FS}
4	1.4

Table3-2-4 Fitting parameters of ITO film 961.6nm

ω_p(rad.THz)	τ(fs)	μ(cm^2/Vs)	N(cm^{-3})
1950	6.4	32.2	4.2×10^{20}

In the Table3-2-1, ε_∞ is the high frequency dielectric constant. n_{FS} is the refraction index of fused silica in this spectral range.

In the Table3-2-2, 3-2-3, and 3-2-4, the mobility is calculated from $\mu=e\tau/m^*$, where $m^* = 0.35\ m_e$ [21] is the effective mass of ITO. N is the carrier concentration that satisfied $N= \omega_p^2 m^* \varepsilon_0/e^2$, where e is the electron charge with unit coulomb.

In Fig.3-2-3 to 3-2-5, we find out that there are two resonate peak in the period from $30 \sim 37.5$THz (i.e. 8µm to 10µm). It is the signature of our ITO film [21], but we did the fitting without including these futures. In order to compare the reflection spectra with Drude formula, we neglected the phenomenon. And the fitting range is from 12 THz to 225 THz (i.e. 400 cm^{-1} to 7500 cm^{-1}).

In summary, we get the results similar to the Hall measurement by Drude free electron model fitting. And Drude model works very well for the whole spectrum except the unknown resonance. In conclusions, the plasma frequency is increasing as the thickness increasing in the view of frequency (the unit of x-axis is Hz). The carrier concentration has the same behavior. And the mobility is in the range of Hall measurement. As result, the carrier scattering time is comparable to the literature [27].

Table3-2-5 Fitting parameters of ITO film, 961.6nm, 483.0nm, and 188.9nm

compare with the Hall measurement.

FTIR	ω_p(THz)	τ(fs)	μ (cm^2/Vs)	N (cm^{-3})	σ_0 (Ω^{-1}cm^{-1})	R_s ($\Omega/\square$)
Film: 188.9(nm)	1600	6.8	34.2	2.8×10^{20}	1532	34.6
Film: 483.0(nm)	1860	6.7	33.7	3.8×10^{20}	2049	10.1
Film: 961.6(nm)	1950	6.4	32.2	4.2×10^{20}	2164	4.8
Hall						
Film: 188.9(nm)			38.4	-2.5×10^{20}	1557	34.03
Film: 483.0(nm)			38.0	-3.4×10^{20}	2045	10.1
Film: 961.6(nm)			34.3	-4.1×10^{20}	2250	4.62

In table 3-2-5, we also can find out that the DC conductivity and the sheet resistivity are comparable to the electrical measurement.

3-3 THz Time Domain Spectroscopy
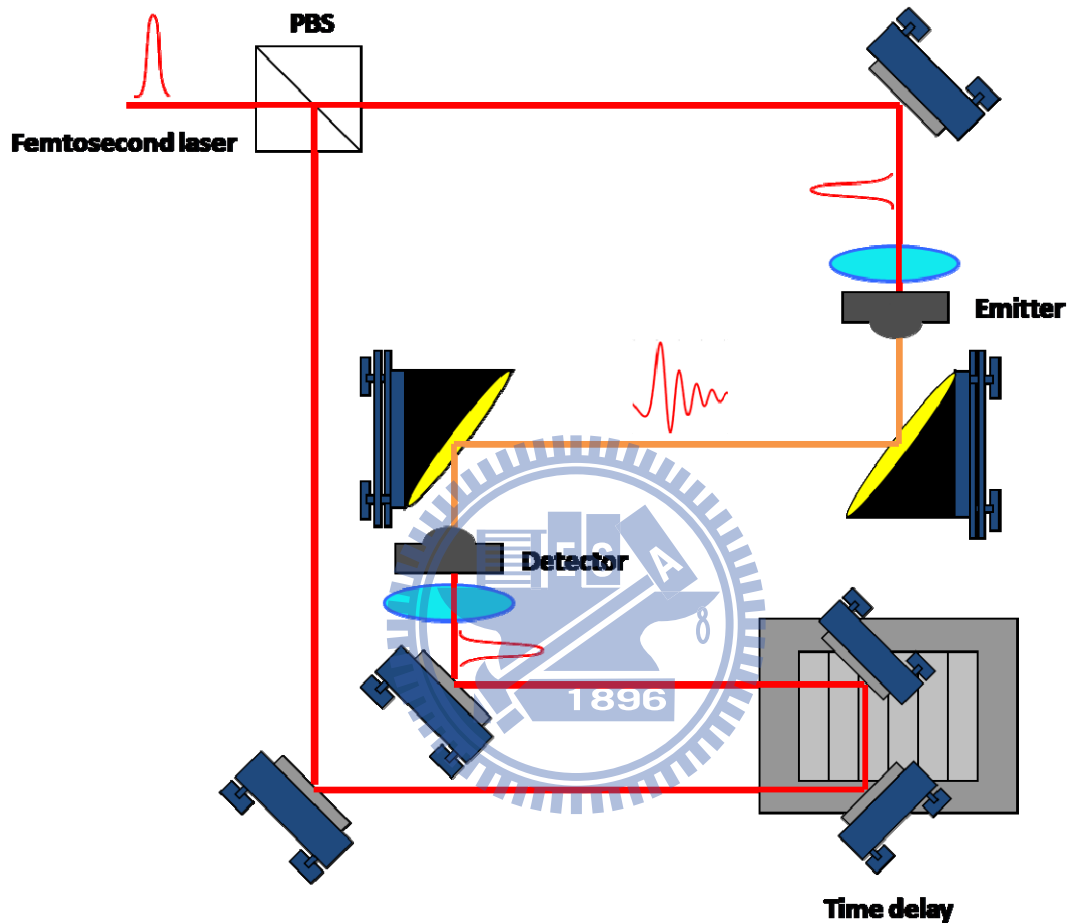
System Set Up (Transmission Type)

Fig.3-3-1 Antenna THz time domain spectroscopy system

It is an optical pump probe system with the pulse duration, 50fs, the center wavelength, 800nm, and the repetition rate, 80MHz. The emitter and the receiver are composed by GaAs. And the THz pulse width was 1ps with a frequency domain spectrum 0.15 ~ 3THz. We purged the system with the nitrogen when we were measuring.

Data Analysis

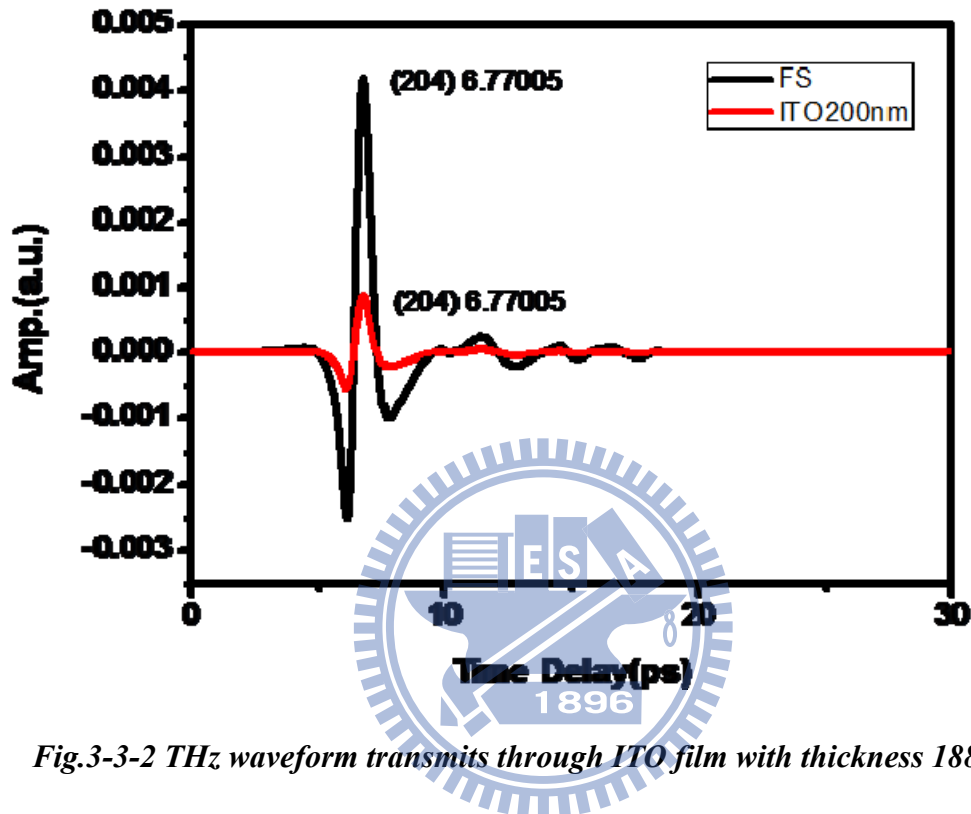**ITO FILM (FS) : 188.9nm (10µm per step)**

Fig.3-3-2 THz waveform transmits through ITO film with thickness 188.9nm.

The lower one is the signal for ITO film, and the higher one is the reference for the fused silica. In the Fig.3-3-2, we find out that the peak positions are at the same delay time. That is because the sample is very thin. Therefore, in the time domain waveform, we cannot distinguish the reference peak position and the signal peak position with the delay resolution, 10µm.　Note here: the delay stage of the system steps 1µm. The corresponded delay time to the time domain spectroscopy is 2µm.
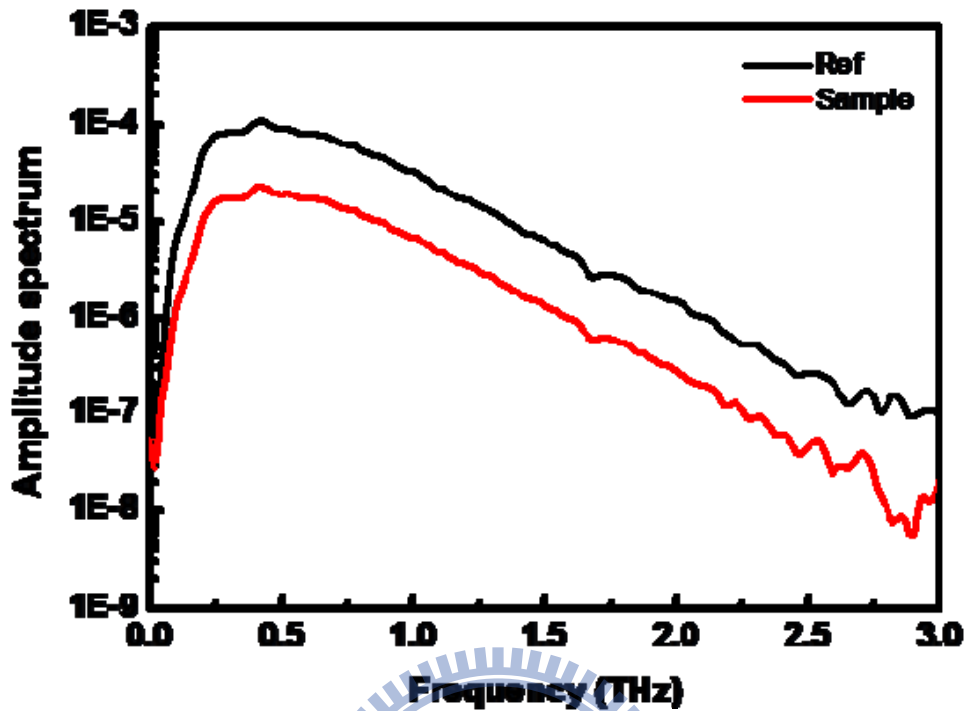
Fig.3-3-3 THz frequency domain spectra of TO film with thickness 188.9nm

The lower one is the signal for ITO film, and the higher one is the reference for the fused silica. With the frequency domain spectroscopy, we could derive out the refractive index. It is because the absorption of the ITO thin film is very obvious. Note here: with the nitrogen purge, we have the frequency domain spectrum above. There are almost no water absorption peaks in the spectrum. It will make our analysis to be more convinced.
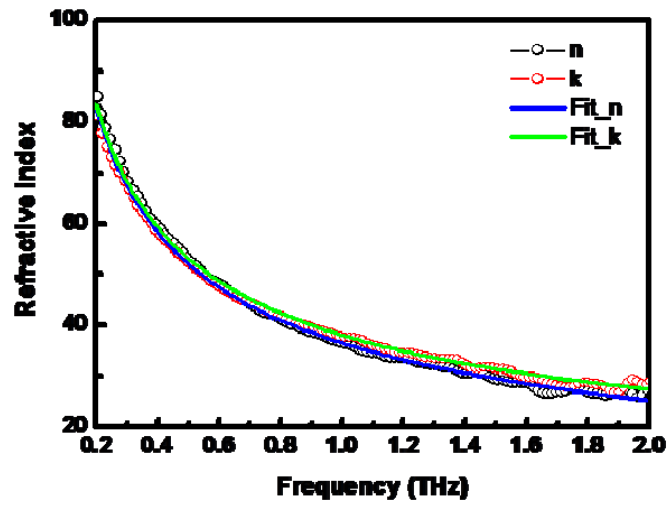
Fig.3-3-4 The refraction index of TO film with thickness 188.9nm.

κ value is larger than n value at the high frequency part, and they are going to become close at the low frequency part.
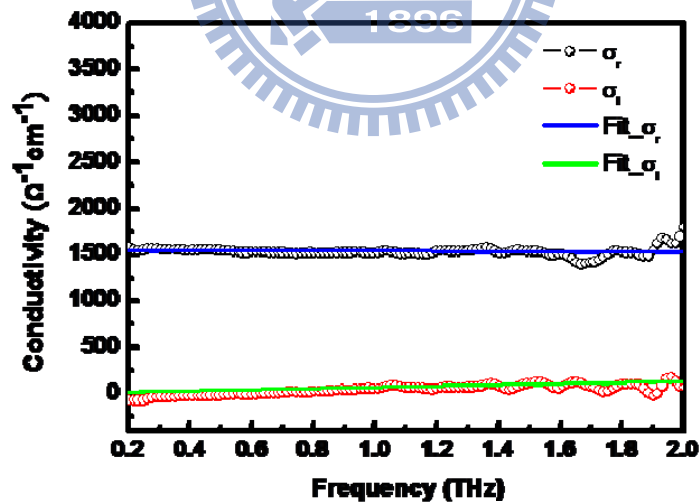

Fig.3-3-5 σ(ω) of TO film with thickness 188.9nm

It shows the Drude model like behavior. Therefore we fit the data with Drude free electron model.
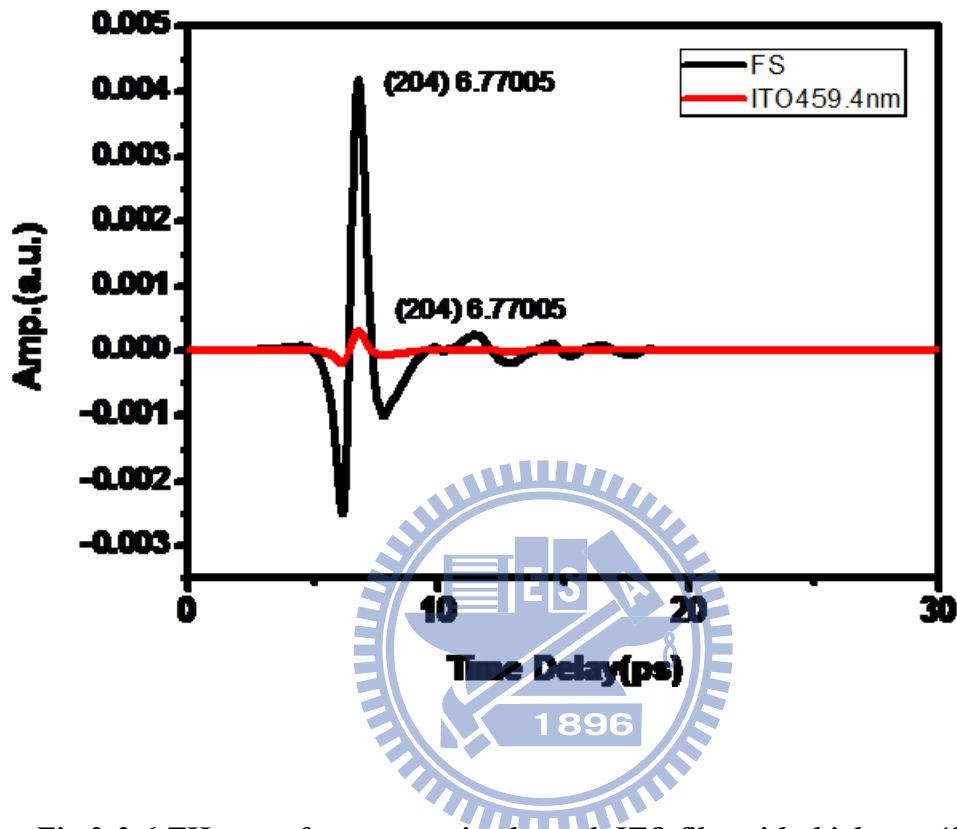
ITO FILM (FS) : 483.0nm (10μm per step)

Fig.3-3-6 THz waveform transmits through ITO film with thickness 483.0nm.

The lower one is the signal for ITO film, and the higher one is the reference for the fused silica. In the Fig.3-3-6, we can also find out that the peak positions are at the same delay time. That is because the sample too thin to distinguish the reference peak position and the signal peak position with the delay resolution, 10μm.
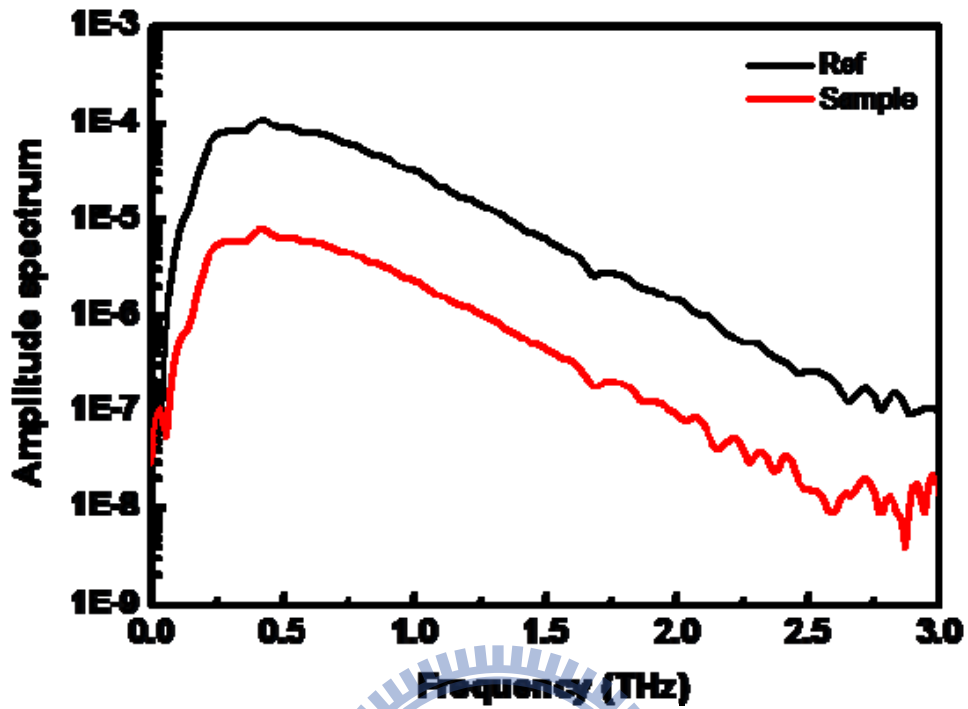
Fig.3-3-7 THz frequency domain spectra of TO film with thickness 483.0nm

The lower one is the signal for ITO film, and the higher one is the reference for the fused silica. With the frequency domain spectroscopy, we could derive out the refractive index. It is because the absorption of the ITO thin film is very obvious. Note here: with the nitrogen purge, we have the frequency domain spectrum above. There are almost no water absorption peaks in the spectrum. It will make our analysis to be more convinced.
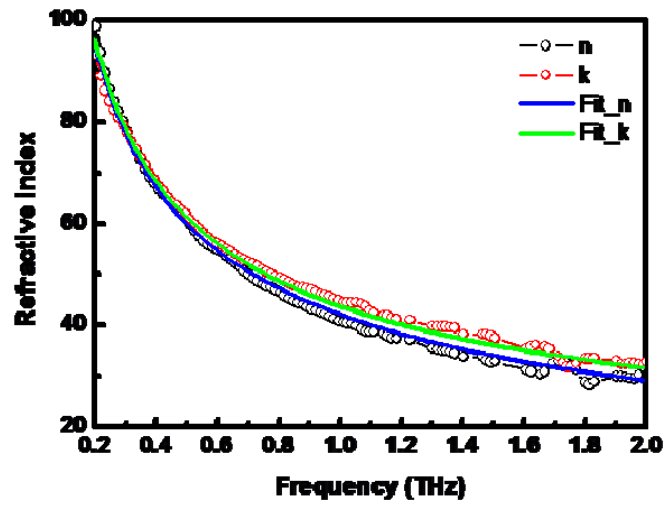
Fig.3-3-8 The refraction index of TO film with thickness 483.0nm

κ value is larger than n value at the high frequency part, and they are going to become close at the low frequency part.
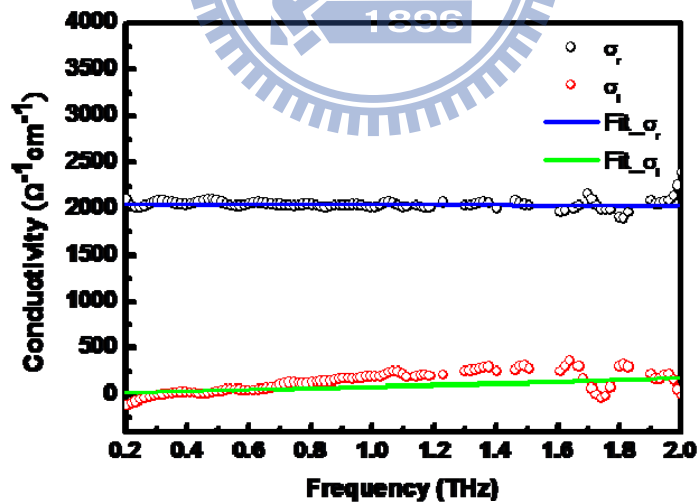

Fig.3-3-9 σ(ω) of TO film with thickness 483.0nm

It shows the Drude model like behavior. Therefore we fit the data with Drude free electron model.

ITO FILM (FS) : 961.6nm (10μm per step)

Fig.3-3-10 THz waveform transmits through ITO film with thickness 961.6nm.

The lower one is the signal for ITO film, and the higher one is the reference for the fused silica. In the Fig.3-3-10, the peak positions of the reference and the signal are separated. It means that with the time resolution fixed at 10μm. We could distinguish the peak position of the reference and the signal as the thickness of ITO thin film up to 1μm. In the figure, we also can find out that the difference of them is only one step.
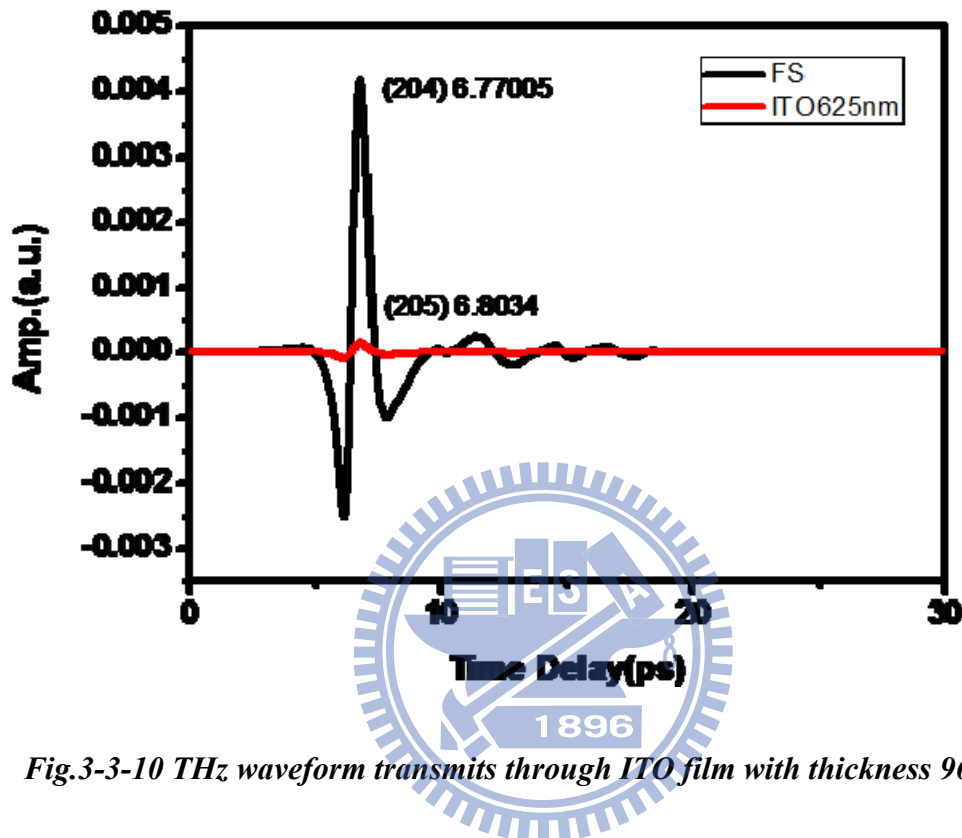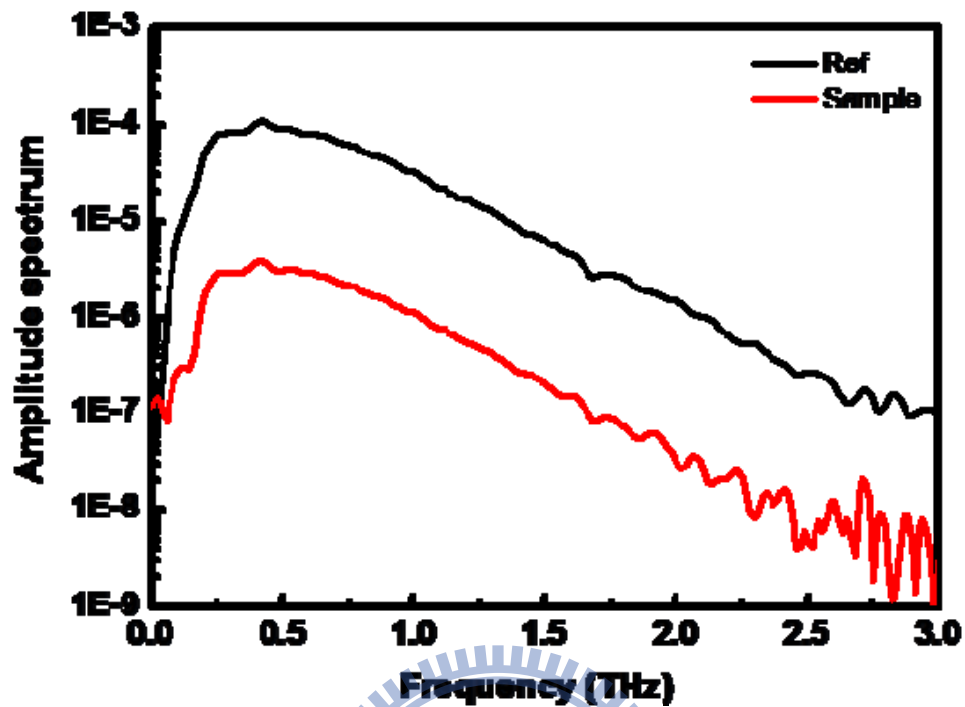
Fig.3-3-11 THz frequency domain spectra of TO film with thickness 961.6nm

The lower one is the signal for ITO film, and the higher one is the reference for the fused silica. With the frequency domain spectroscopy, we could derive out the refractive index. It is because the absorption of the ITO thin film is very obvious. Note here: with the nitrogen purge, we have the frequency domain spectrum above. There are almost no water absorption peaks in the spectrum. It will make our analysis to be more convinced. But in the high frequency range, the signal and noise ratio is smaller. Therefore, the analysis is limited by the SN ratio of the spectrum.
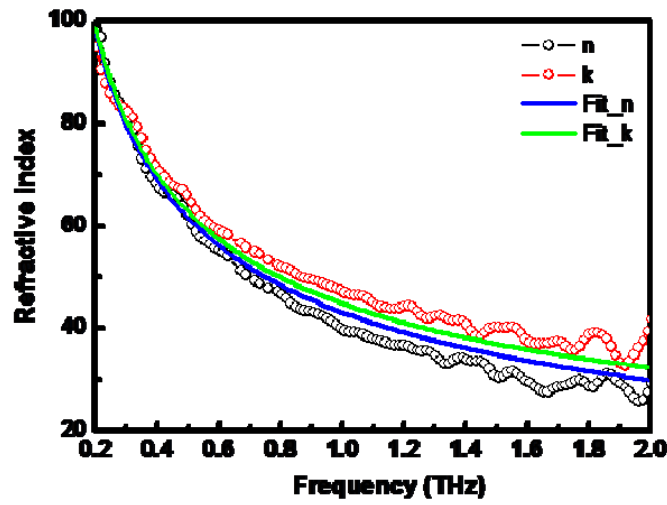
Fig.3-3-12 The refraction index of TO film with thickness 961.6nm

κ value is larger than n value at the high frequency part, and they are going to become close at the low frequency part.
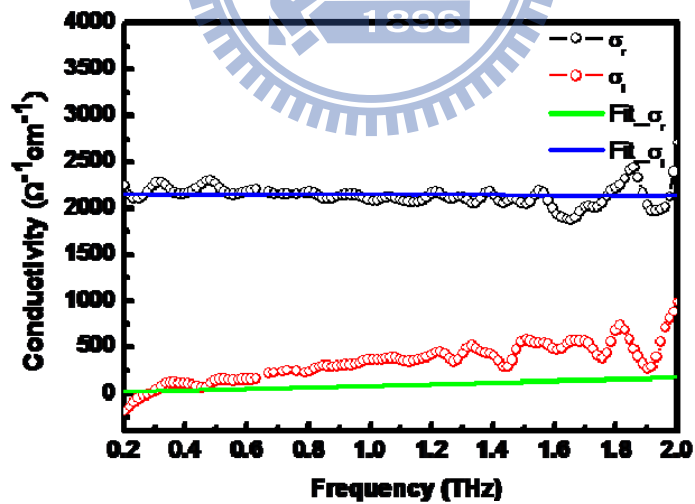
Fig.3-3-13 σ(ω) of TO film with thickness 961.6nm

It shows the Drude model like behavior. Therefore we fit the data with Drude free electron model.

Fig.3-3-14 Compared the frequency domain spectra of the ITO thin films

Fig.3-3-15 Compared the refractive index of the ITO thin films

Fig.3-3-16 Compared the conductivity of the ITO thin films

From the left to the right, they are following the rule, 188.9nm, 483.0nm, and 961.6nm, respectively.

In the Fig.3-3-14, we find out the amplitude of the frequency domain spectra becoming lower as the thickness growing up. And it will cause the SN ratio to be bad. Therefore, the usage spectrum will become smaller with the sample thickness increasing.

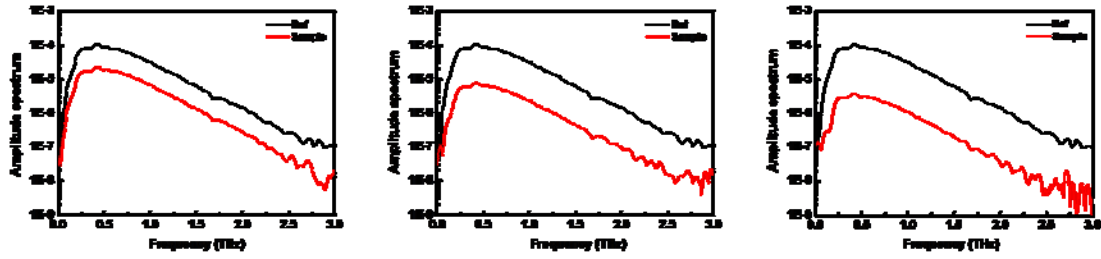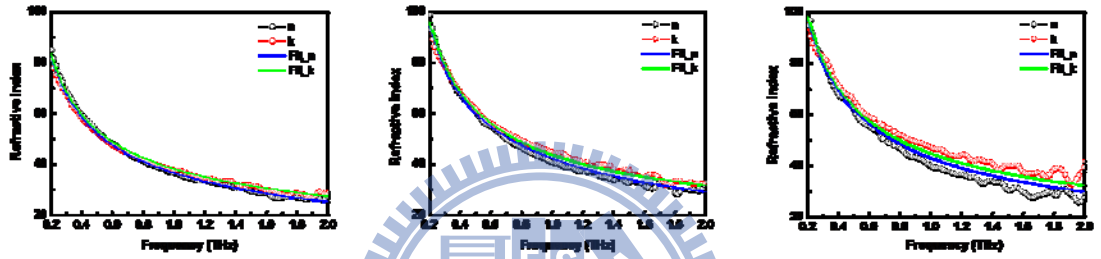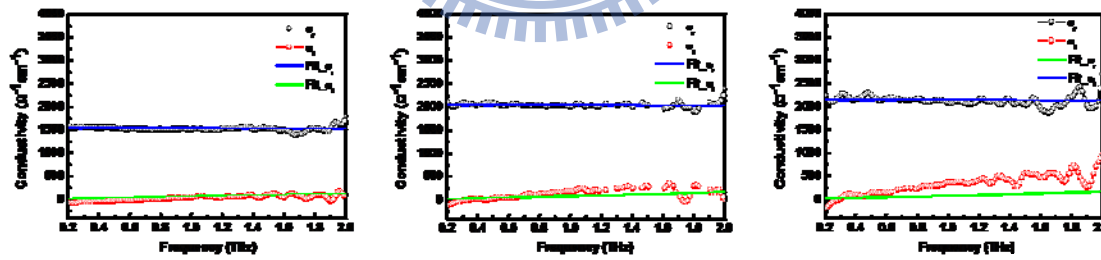In the Fig.3-3-15, we find that as the thickness increasing the refractive index is also increasing. But the value of the real part refractive index cannot be told from the time domain spectroscopy. It is because the signal is mixing so much frequency and it is the result of multibeam interference. We cannot tell the difference between the reference and the signal for the thin sample with the long time delay. And in the literature [28], the refractive index of ITO thin film at THz range is similar to our results.

In the Fig.3-3-16, the real part of the conductivity has become larger as the thickness of sample increasing. And we also find that as the SN ratio becoming badly, we cannot find a suitable result. Therefore, we introduce the parameters of FTIR into the THz-TDS analysis to recheck the data.

The plasma frequency of ITO film is far away from our light source spectrum. If there is a little vibration in $\sigma(\omega)$, it will mislead the fitting parameters that cannot extract the exact optical and electrical constants. Therefore, we introduce the plasma frequency calculated from FTIR into our conductivity fitting to recheck the optical measurement properties.

Table 3-3-1 Compared THz-TDS, Hall, and FTIR with the optical and electrical parameters

THz-TDS	ω_p (rad.THz)	τ (fs)	μ (cm^2/Vs)	N (cm^{-3})	σ_0 ($\Omega \cdot$cm)	R_s ($\Omega/\square$)
Film: 188.9(nm)	1600	6.8	33.9	2.8×10^{20}	1519	34.9
Film: 483.0(nm)	1860	6.7	33.8	3.8×10^{20}	2055	10.1
Film: 961.6(nm)	1950	6.5	32.4	4.2×10^{20}	2177	4.8
Hall						
Film: 188.9(nm)			38.4	-2.5×10^{20}	1557	34.03
Film: 483.0(nm)			38.0	-3.4×10^{20}	2045	10.1
Film: 961.6(nm)			34.3	-4.1×10^{20}	2250	4.62
FTIR						
Film: 188.9(nm)	1600	6.8	34.2	2.8×10^{20}	1532	34.6
Film: 483.0(nm)	1860	6.7	33.7	3.8×10^{20}	2049	10.1
Film: 961.6(nm)	1950	6.4	32.2	4.2×10^{20}	2164	4.8

In table 3-3-1, the parameters from different measurements are comparable to each other. And the results are similar to the literatures. For example, the scattering time is around 10fs. The results are also close to the Hall measurement.

Compared the result of the optical measurement and the electrical measurement is shown below: Indeed, the results are very close to each other because of the grain size of ITO film is larger than the carrier mean free path of ITO. [29]

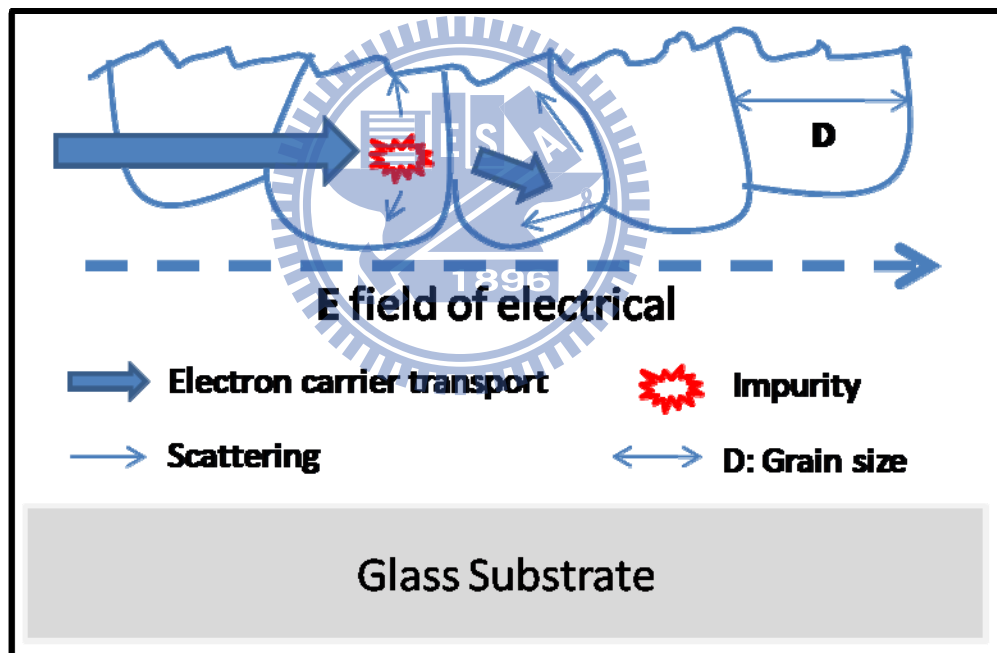**The physical diagrams of our measurement**

Fig.3-3-17 The physical diagram of electrical measurement
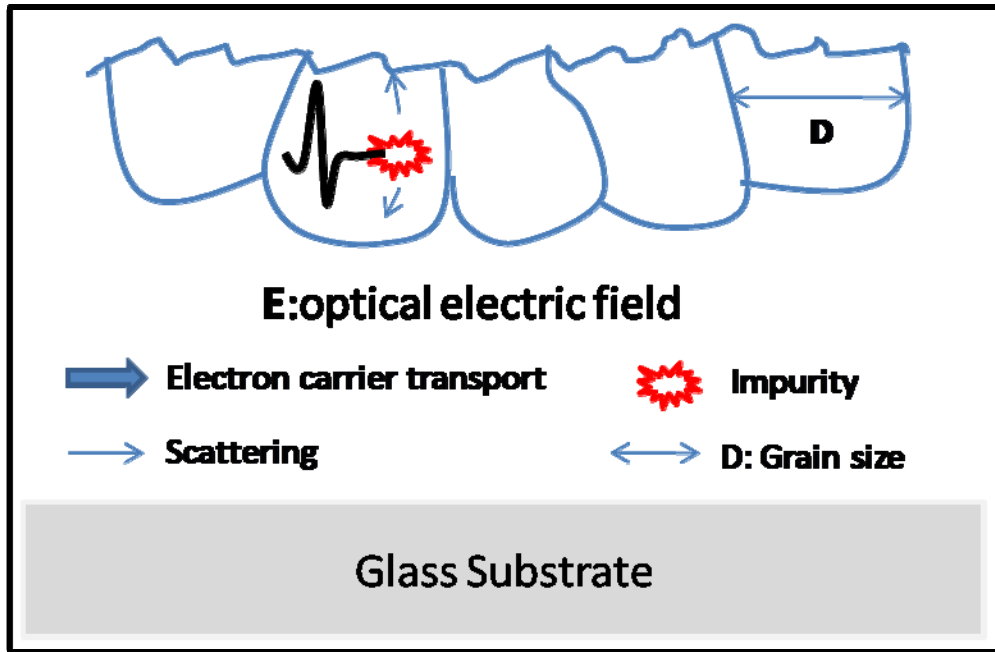
Fig.3-3-18 The physical diagram of optical measurement

We can find out that the electrical measurement will affect by the grain boundary scattering. On the other hand, optical measurement won't affect by the grain size when the optical frequency is high enough. In our case, the mean free path of ITO film is below 5nm [21] which is smaller than the grain size calculated from SEM. Therefore, we shall have the same results as the intra-grain scattering dominate with optical measurement and electrical measurement.

Chapter 4 : ITO nanocolumn characterization

4-1 Characters of ITO nanocolumn and motivations

ITO nanocolumn (with N$_2$ flux)
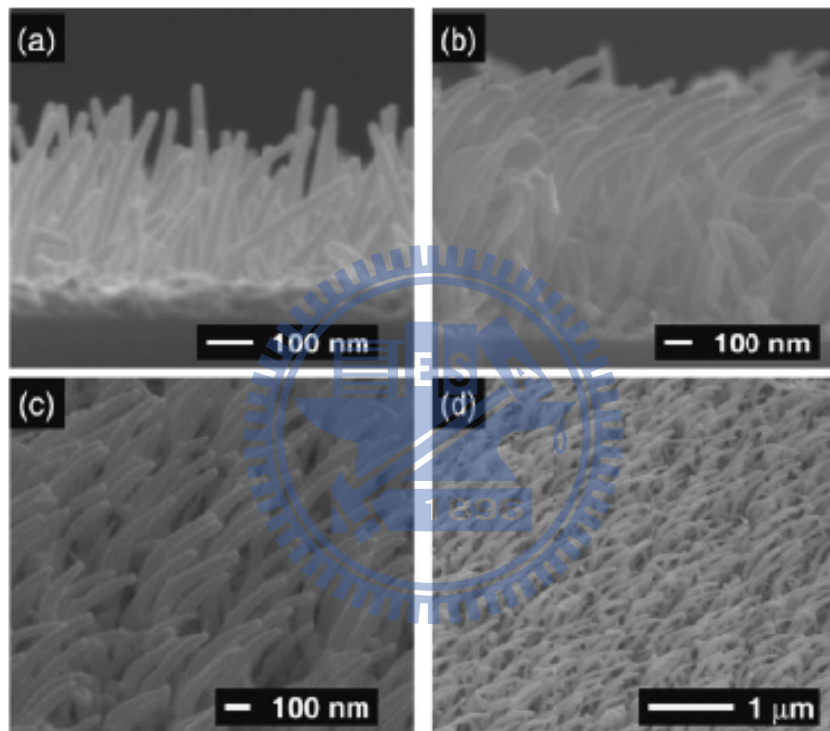
Fig.4-1-1 SEM of ITO nanocolumn [15]

The spectroscopy of ITO at the visible range (300nm to 900nm) for both s- and p- polarized wave incidence are relatively low, respectively. With the gradient index structure and less dense ITO material on the substrate, it causes highly transparent. And to be a good TCO, the sheet resistivity is an important topic for being concerned. However, electrical method such as Hall measurement will destroy the sample surface. Therefore, we need a non contact method to determine the electrical properties of the ITO nanocolumn.

4-2 Data Analysis

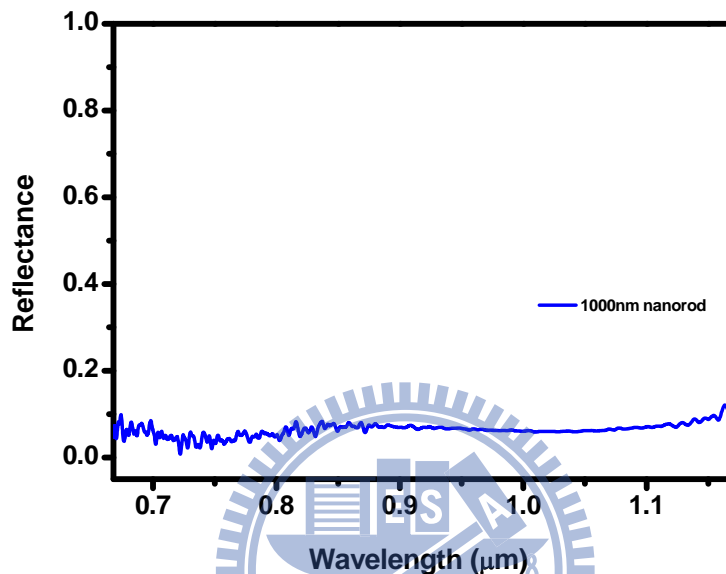**FTIR spectroscopy**

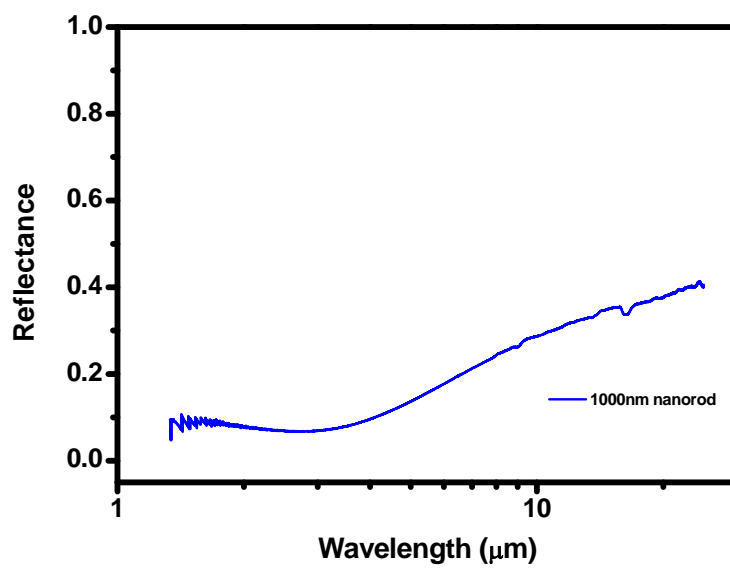***Fig.4-2-1 FTIR of ITO nanocolumn at low wavelength part***

Fig.4-2-2 FTIR of ITO nanocolumn at high wavelength part

The FTIR spectra were recorded using "Bomen da8.3" spectrometer by Instrument Center at National Tsing Hua University. The angle of incidence is 18° related to the sample normal. A ratio of the single beam spectra of ITO films to a single beam spectrum of a planar gold mirror was performed to obtain the reflectance spectra of ITO films with a 6mm hole to confine the detection range. The whole spectra cover from 0.6μm to 71.6μm (i.e. 15000cm^{-1} to 140cm^{-1}).

FTIR data fitting

We introduce effective medium theory to our dielectric function because of it is a nanostructure sample. In the following analysis, we use the Bruggeman assumption to deal with the ITO nanocolumn. We have the dielectric function as followed:

$$\varepsilon = 1 \times [1-F] + F \times \left[\varepsilon_\infty - \frac{\sigma}{i\omega\varepsilon_0} + \frac{S \times \omega_p^2}{\omega_p^2 + \omega^2 - i\Gamma\omega} \right], F = 0.32 \quad \text{--- (4-1-1) [20]}$$

It can be derived from the Clausius-Mossotti relation with two phase mixtures. And F, the fraction of the occupying volume for the ITO nanocolumn, is determined by the SEM.

The substrate of ITO nanocolumn is silicon. Considering the refraction index of it around this range (15000cm-1 to 140cm-1), we took it as a constant, nsub = 3.42. And we use the Drude Smith model to calculate the electrical properties.

$$\widetilde{\sigma}(\omega) = \left(\frac{\varepsilon_0 \omega_p^2 \tau}{1-i\omega\tau} \right)[1 + \frac{c}{1-i\omega\tau}]; \quad \text{--- (4-1-1) [17]}$$

ITO Rod (Si) : 1μm
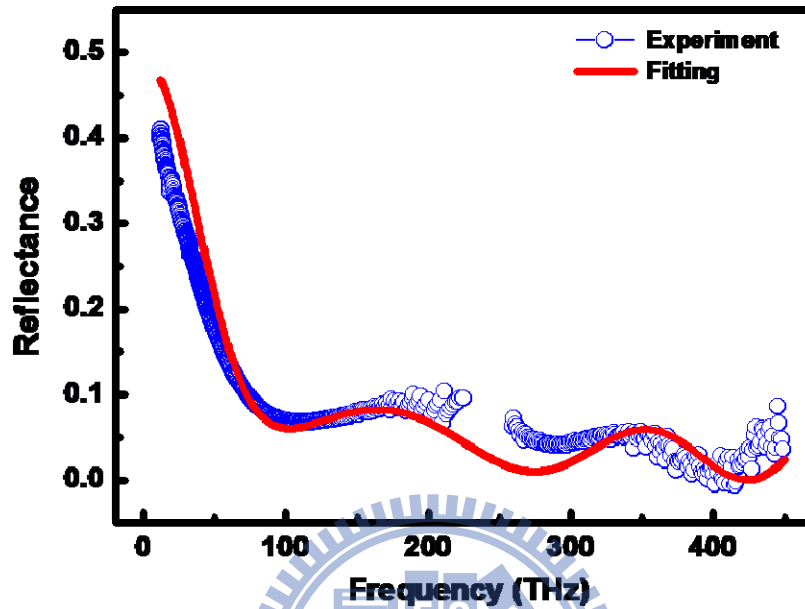
Fig.4-2-3 Fitting curve of ITO nanocolumn

Table 4-2-1 fixed value

d (nm)	f
700	0.32

Table 4-2-2 Calculated from the model fitting of FTIR

Sample	ω_p (rad.THz)	τ (fs)	c	μ (cm²/Vs)	N (cm⁻³)	σ_0 (Ω^{-1}cm⁻¹)
ITO nanocolumn	3200	0.7	-0.6	1.4	1.1×10^{21}	254

THz-TDS: (Transmission Type)

ITO Rod (Si) : 1µm (2µm per step)

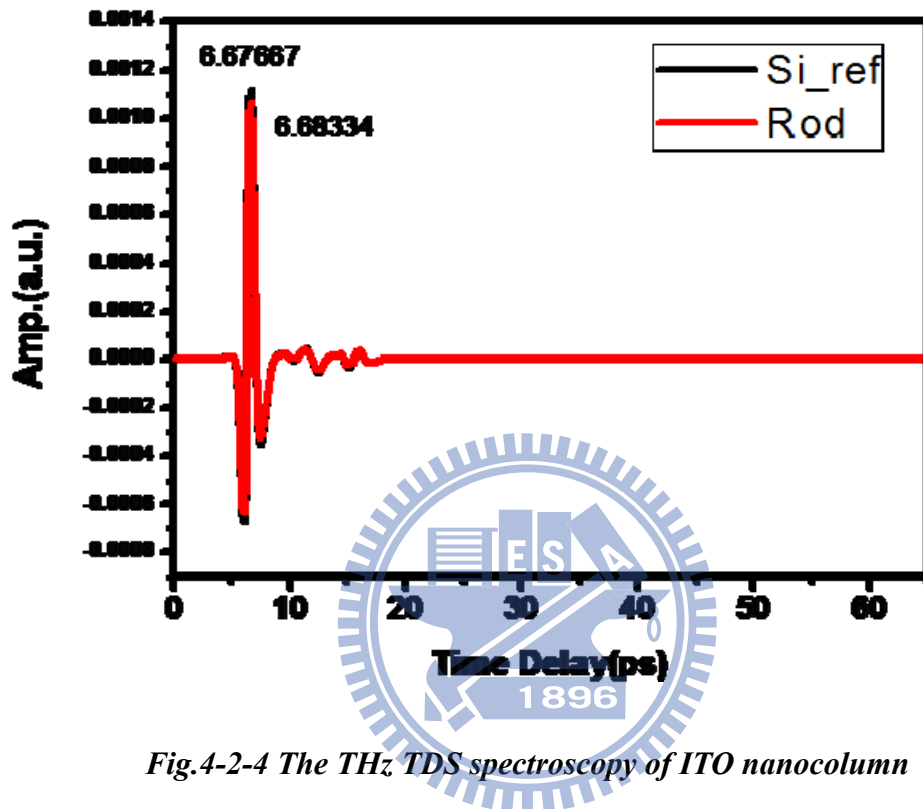*Fig.4-2-4 The THz TDS spectroscopy of ITO nanocolumn*

The higher one is the reference data and the lower one is the signal data. In the Fig.4-2-4, we can find out that the amplitude transmission is close to 100%. Therefore, we have to set the higher time resolution to demonstrate our experiment. The reference waveform and the signal waveform are determined with the time delay, 2µm per step. With this condition, we could tell the difference between them.
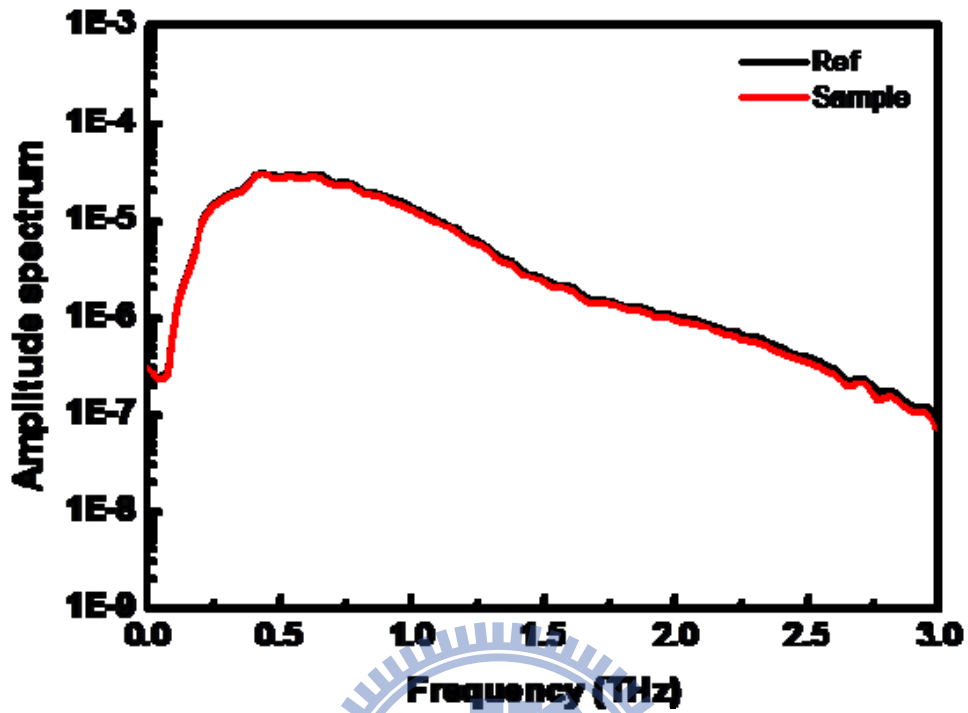
Fig.4-2-5 The frequency domain spectroscopy of ITO nanocolumn

The higher one is the reference data and the lower one is the signal data. And we have the result is that the amplitude spectra in frequency domain are almost the same for the reference and the signal data. It means that the imaginary part of the refractive index will be very small or there are not many actions between the propagation light and the sample. The reason might be that the sample, ITO nanocolumn, is growth on substrate with rare part. The fraction of the nanocolumn to the tatol volume is 0.32. It will cause less absorption.
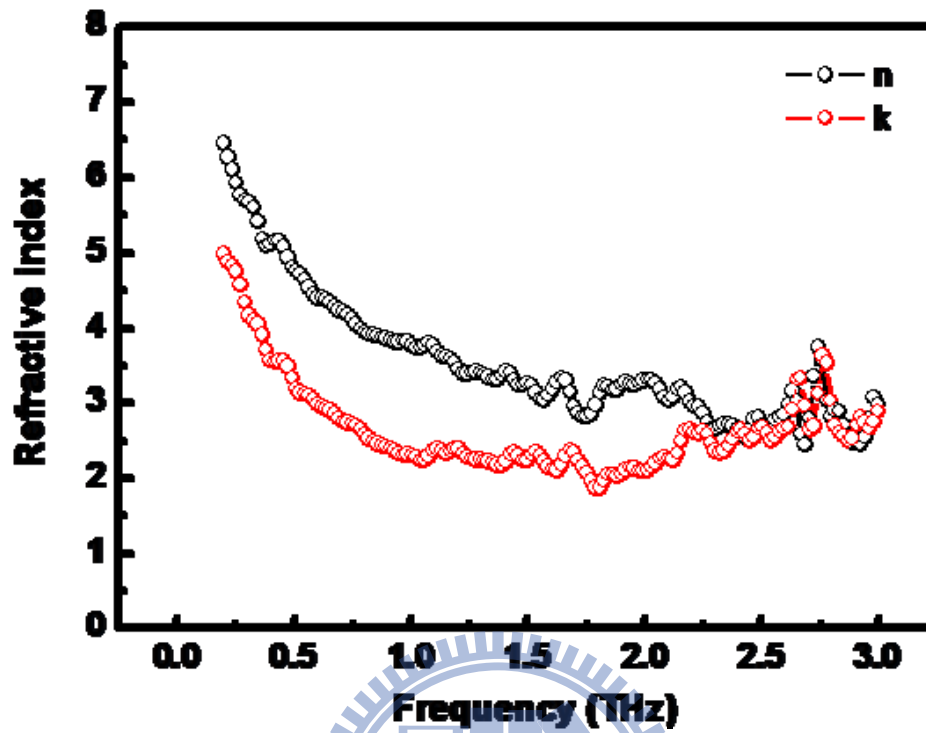
Fig.4-2-6 The refraction index of ITO nanocolumn in THz range

The higher one is n and the lower one is κ. We can easily find out that the imaginary part of the refractive index is relatively low to the value of ITO films. There are much noises at high frequency part with unknown phenomenon occurred.
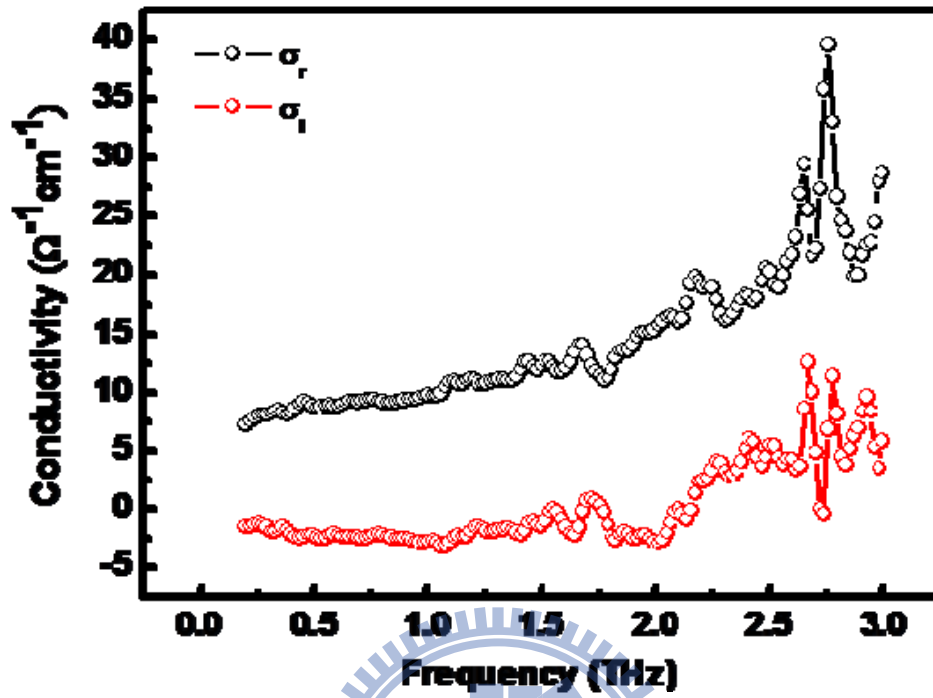
Fig.4-2-7 The $\sigma(\omega)$ of ITO nanocolumn in THz range

The higher one is the real part and the lower one is the imaginary part. The conductivity is relatively low to the ITO thin film. And it means that their behavior will totally different at the THz range. We also can find out there are strong vibrations at high frequency range.

In the FTIR analysis, we find that the mobility and the conductivity are lower than the thin film structure. And then, the sheet resistivity, ∼ 56(Ω/□), is higher than the thin film sample. For a good TCO, the sheet resistivity should below 10(Ω/□).

In the THz-TDS analysis, we also introduced effective medium theory into our analysis in THz TDS data. In the Fig.4-2-4, Fig.4-2-5, we find that the transmission is very high, about 90%. Therefore, we have to compare them, both THz-TDS and FTIR.

Discussion: Comparison of THz-TDS and FTIR measurements

In Fig.4-2-3, the reflectance of nanocolumn is gradually increasing as the frequency going smaller. For this reason, low transmittance should be found at low frequency range, especially in the range of our THz-TDS system. Unfortunately, the result is opposite. Hence, there must have physical phenomena occurring in the range, from 2 THz to 11 THz. By plotting the refraction index and the conductivity with the parameters extracted from FTIR fitting, we found that the values what we recalculated were higher than the THz-TDS measurement.
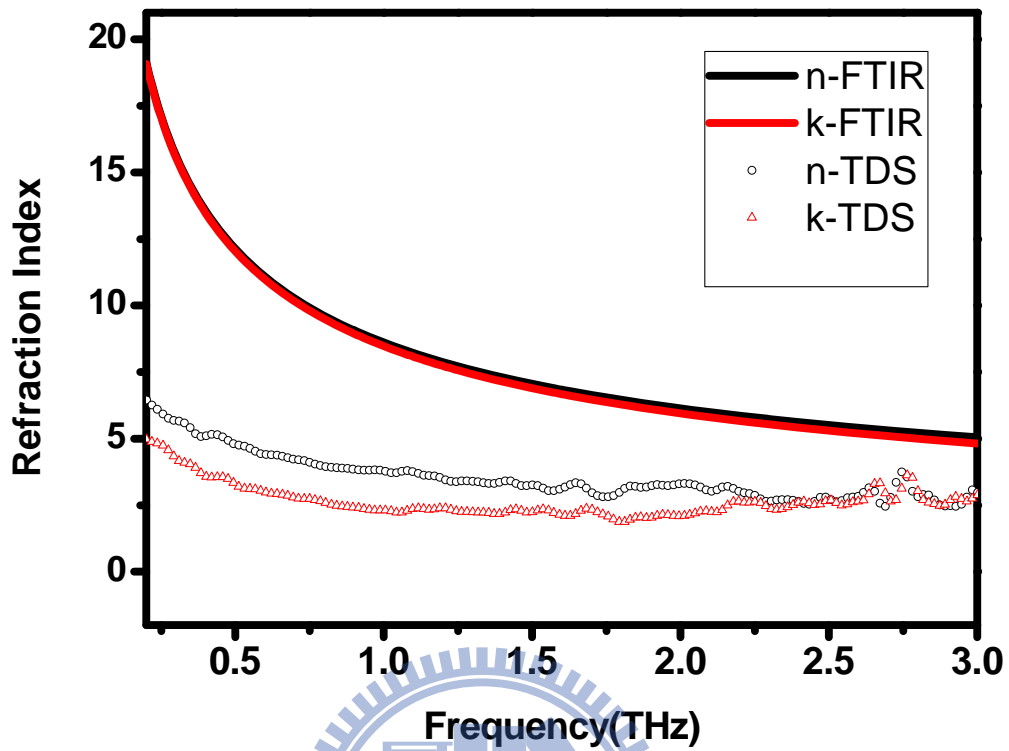
Fig.4-2-8 Refraction index of ITO nanocolumn from FTIR and THz-TDS

The refraction indices of FTIR differ from the one got from THZ-TDS. For FTIR, it is similar to a conductor at low frequency range because the n κ values become close.
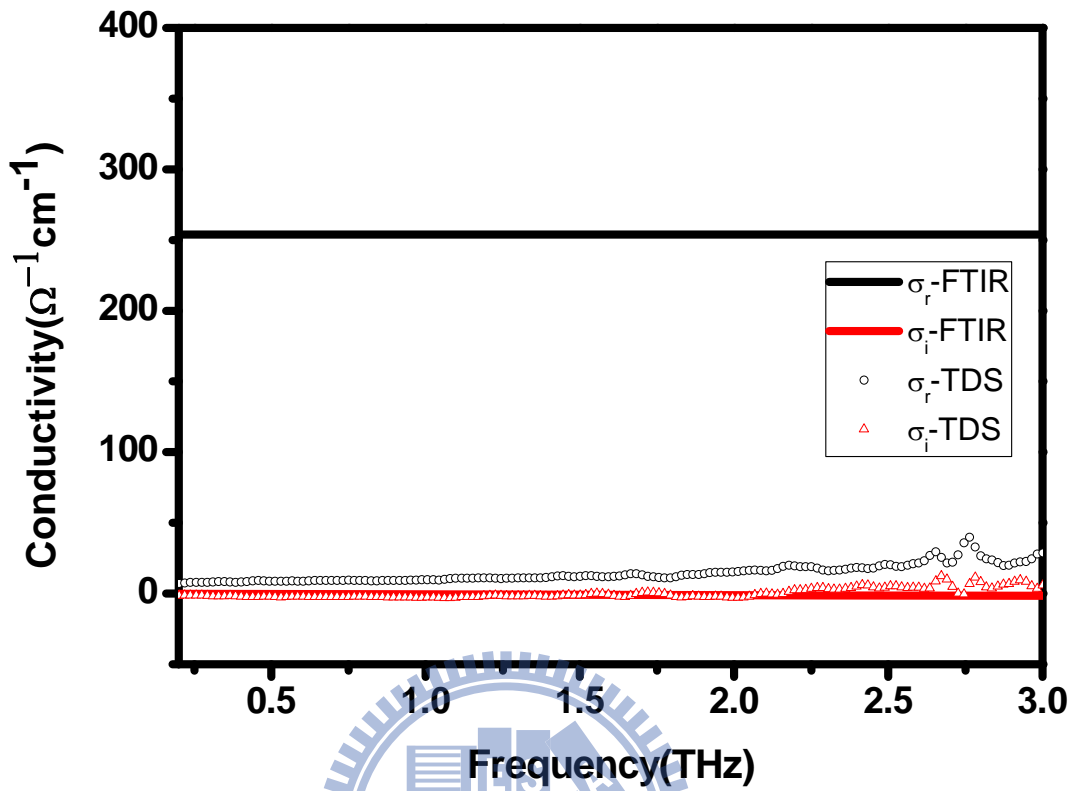
Fig.4-2-9 Conductivity of ITO nanocolumn from FTIR and THz-TDS

Conductivity calculated from FTIR is larger than the TDS one. The real part of the conductivity from the FTIR is larger than the THz-TDS calculation for the ITO nanocolumns. For the FTIR conductivity at THz range, it is not directly determined by the far infrared light source. It is just a fitting process to have the conductivity cover to the THz range. And it is weird that the two experiments have the different results. Therefore, there are something happened around 3THz.

Without enough evidences, we cannot give a conclusion which is right or wrong. Nevertheless, the parameters extracted from FTIR must close to the correct number because the fitting range is far from the unexpected phenomena. And we guess the phenomenon is the phonon resonance at several THz. It causes us to find another term to fit the data, but it doesn't finish yet. The physical meanings of the phenomena were discussed in Chapter 2. The topic is "propagation of light in isotropic dielectrics".
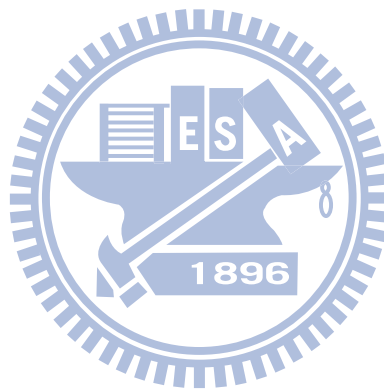
Chapter 5 : Conclusion

We demonstrate the optical characterization methods including FTIR and THz-TDS to investigate the electrical properties of the ITO thin film and ITO nanocolumn. For different thicknesses of the ITO thin films (189nm~961nm), the plasma frequencies are determined to be from 1600 (rad.THz) to 1950 (rad.THz), and scattering time are in the range of 6~7 fs based on the free electron Drude model. The mobility is obtained to be 32~34cm^2/Vs. The carrier concentration is verified to be in the range of (2.8~4.2)×10^{20}. These electrical properties of ITO thin film samples, which are derived from the non-contact optical techniques, agree well with that determined by the conventional Hall measurement.

Moreover, the novel and superior optical technique are applied to perform the characterization of ITO nanocolumn, which is the popular material used in the photovoltaic applications. A proposed dielectric function associated with Drude-Smith model is reported in this study. Further work and discussions are under. More thorough research is in the middle of advance at present.

Reference:

[1]   Auston DH,   Appl. Phys. Lett., Vol. 45, pp. 284, 1984.

[2]   Rice A. et al., Appl. Phys. Lett., Vol.64, pp. 1324, 1994.

[3]   X.-C. Zhang, Appl. Phys. Lett., Vol. 56, pp. 1011, 1990.

[4]   R. Kohler et al., Nature, Vol. 417, pp. 156, 2002.

[5]   Q. Wu, Appl. Phys. Lett., Vol.6, pp. 3523, 1995.

[6]   A.G. Markelz, Chem. Phys. Lett., Vol. 320, pp. 42, 2000.

[7]   B.B. Hu, Opt. Lett., Vol. 20, pp. 1716, 1995.

[8]   D. Grischkowskey, J. Opt. Soc. Am. B, Vol. 7, No. 10, pp. 2006, 1990.

[9]   M. Van Exter, Appl. Phys. Lett., Vol. 56, pp. 1694, 1990.

[10]   M.C. Beard, Nano. Lett., Vol. 3, pp. 1695, 2003.

[11]   Jason B., J. Phys. Chem. B, Vol. 110, pp. 25229, 2006.

[12]   D. G. Cooke, Phys Rev. B, Vol. 73, pp. 193311, 2006.

[13]   Joachim Muller, Solar Energy, Vol. 77, pp. 917, 2004.

[14]   A. Shah, Thin Solid Films, Vol. 502, pp. 292, 2006.

[15]   Peichen Yu, Adv. Mater., Vol. 21, pp. 1, 2009.

[16]   Grant R. Fowles, "Introduction to Modern Optics," Second Edition.

[17]   N.V. Smith, Phys Rev. B, Vol. 64, pp. 155106, 2001.

[18]   N. W. Ashcroft, "Solid State Physics," Saunders College Publishing, Philadephia, 1976.

[19]   Charles Kittel, "Introduction to Solid State Physics," Seventh Edition.

[20]   P.J.B. Clarricoats, "Electromagnetic Mixing Formulas and Applications," IEE Electromagnetic Waves Series 47.

[21]   I. Hamberg, J. Appl. Phys., Vol. 60, pp. R123, 1986.

[22]   Ho-Chul Lee, Vacuum, Vol. 80, pp. 880, 2006.

[23]   Zhaohui Qiao, Thin Solid Films, Vol. 496, pp. 520, 2006.

[24]   J. Steinhauser, Appl. Phys. Lett., Vol. 90, pp. 142107, 2007.

[25]   I. Hamberg, Appl. Phys. Lett., Vol. 40, pp. 362, 1982.

[26]   D. Mergel, J. Phys. D: Appl. Phys., Vol. 35, pp. 794, 2002.

[27]   Scott H. Brewer, J. Phys. Chem. B, Vol. 106, pp. 12986, 2002.

[28]   S.A. Jewell, New Journal of Physics, Vol. 10, pp. 033012, 2008

[29]   J. Steinhauser, Appl. Phys. Lett., Vol. 90, pp. 142107, 2007.